LBL-32692
UC-404

Lawrence Berkeley Laboratory
UNIVERSITY OF CALIFORNIA

Engineering Division

To be published in *Encyclopedia of Applied Physics*,
George L. Trigg, editor, VCH Publishers and American Institute of
Physics, Brooklyn, NY

Germanium

W.L. Hansen and E.E. Haller

November 1992

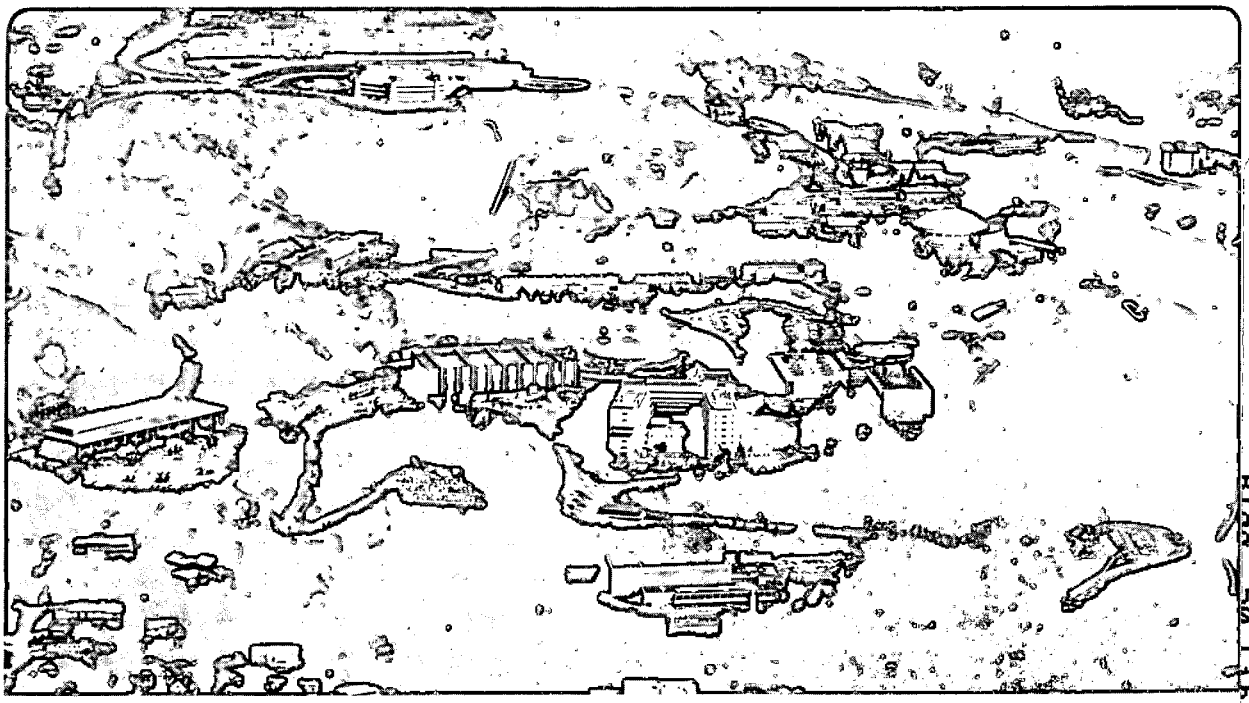

REFERENCE COPY
Does Not
Circulate
Bldg. 50 Library
LBL-32692
Copy 1

Prepared for the U.S. Department of Energy under Contract Number DE-AC03-76SF00098

DISCLAIMER

This document was prepared as an account of work sponsored by the United States Government. While this document is believed to contain correct information, neither the United States Government nor any agency thereof, nor the Regents of the University of California, nor any of their employees, makes any warranty, express or implied, or assumes any legal responsibility for the accuracy, completeness, or usefulness of any information, apparatus, product, or process disclosed, or represents that its use would not infringe privately owned rights. Reference herein to any specific commercial product, process, or service by its trade name, trademark, manufacturer, or otherwise, does not necessarily constitute or imply its endorsement, recommendation, or favoring by the United States Government or any agency thereof, or the Regents of the University of California. The views and opinions of authors expressed herein do not necessarily state or reflect those of the United States Government or any agency thereof or the Regents of the University of California.

LBL-32692

GERMANIUM

W.L. HANSEN and E.E. HALLER*

Lawrence Berkeley Laboratory
University of California
Berkeley, California 94720

and

*Department of Materials Science and Mineral Engineering
University of California at Berkeley

Chapter for the "Encyclopedia of Applied Physics," VCH Publishers
and American Institute of Physics

NOVEMBER 1992

This work was supported by the Director, Office of Energy Research, Office of Health and Environmental Research, of the U.S. Department of Energy under Contract No. DE-AC03-76SF00098.

GERMANIUM

W.L. Hansen and E.E. Haller

Table of Contents

Introduction

1. Physical and Chemical Properties

2. Electronic Properties
- 2.1. Band structure
- 2.2. Impurity and defect levels
- 2.3. Electronic transport
  - 2.3.1. Intrinsic conduction
  - 2.3.2. Extrinsic conduction

3. Optical Properties
- 3.1. Refractive Index and linear absorption coefficient
- 3.2. Photoconductivity
- 3.3. Photoluminescence

4. Technology
- 4.1. Production
- 4.2. Crystal growth
- 4.3. Impurities and defects
  - 4.3.1. Solubility
  - 4.3.2. Segregation coefficient
  - 4.3.3. Impurity diffusion
  - 4.3.4. Defects

5. Applications
- 5.1. Photodetectors
- 5.2. Nuclear radiation detectors
- 5.3. Low temperature Ge thermistors
- 5.4. Optics
- 5.5. Miscellaneous uses

Introduction

The properties of elemental germanium have been more thoroughly studied than any other member of the periodic table, with the possible exception of silicon. In order to review this extensive body of knowledge, various topics have been selected to illustrate the contribution of the study of germanium to semiconductor theory and technology.

The rise and fall of germanium as the commercially most important semiconductor is reviewed, followed by a description of its chemical and physical properties. Figures which summarize experimental and theoretical data have been selected and they cover electronic and optical properties, technology and applications. Germanium purification and crystal growth are described and the more important current uses are listed.

Germanium was first isolated by C. Winkler in 1886 (Winkler 1886) from the mineral argyrodite but had no commercial use until the Second World War (WW II). Efforts to find a suitable material for radar detectors led to an intensive study of the semiconducting properties of germanium and silicon. These studies verified the importance of trace impurities in controlling electrical properties but did not emphasize the importance of crystalline perfection. Due to the different chemical natures of the semiconductors, silicon devices evolved into "cats whisker" detectors and germanium into "high voltage" rectifiers, both being made with polycrystalline material (Torrey and Whitmar 1948).

Immediately after W.W.II Bell Telephone Labs established a solid state division under the direction of W. Shockley and W. Brattain to begin a coordinated research effort by physicists, chemists and engineers with the goal of producing a solid state amplifier. This work led by 1948 to the invention of the point contact transistor (Bardeen and Brattain 1948), the field effect transistor (Shockley and Pearson 1948) and the junction transistor (Shockley 1949). These devices were made from germanium single crystals.

Germanium devices remained dominant during the first decade after the invention of the transistor due mainly to the ease of purification and crystal growth and low temperature processing when compared to silicon (Biondi 1958). However, once high temperature synthesis and processing of silicon was developed, germanium devices were rapidly replaced by silicon in almost all applications. This immediate dominance of silicon was due mainly to the outstanding surface passivating and impurity masking properties of thermally grown SiO_2 films on silicon and to the larger bandgap allowing higher temperature device operation. The thermal oxide GeO_2 on germanium is water soluble and unstable in air.

The crust of the earth contains about 8×10^{-4} wt % germanium, which is 100 times more abundant than silver, but as there are no rich ores, the supply is very price sensitive. A typical price for the past 30 years has been about 600 US$ per kg of pure polycrystalline Ge (1992 US$).

1. Physical and Chemical Properties

Elemental germanium is brittle and harder than glass, a consequence of its purely covalent tetrahedral bonding. The metallic luster is due to the high refractive index and the large free carrier concentration generated by visible light. The electrical conductivity of pure germanium increases with temperature due to the increase in the concentration of thermally generated electrons and holes. Germanium crystallizes from the melt (T_{melt} = 936° C) in the diamond lattice structure with a lattice constant of 5.65 Å. The diamond lattice is a very open structure, resulting in the expansion of germanium by 4.9% upon freezing.

Chemically, germanium reacts as would be predicted by its location in the periodic table: a column IV element located between silicon and tin. The absence of clearly distinguishing chemical properties, together with its high cost, accounts for the

lack of interest by chemists in studying germanium before its unusual electrical properties were discovered.

Germanium is stable in air up to about 500°C. It is not attacked by HCl, HF, H_2SO_4 or strong alkalis. Germanium is dissolved slowly by HNO_3, H_2O_2 and by sodium hypochlorite (laundry bleach) and dissolves rapidly in mixtures containing HF and a strong oxidizer, e.g., HF-HNO_3, HF-H_2O_2 and, when hot, reacts exothermally with Cl_2 to produce $GeCl_4$. Elemental germanium can be melted with negligible reaction in graphite or fused silica containers in a controlled atmosphere (e.g. N_2, H_2, Ar, He, vacuum). The purity of Ge can be found by measuring its resistivity either at room temperature or at liquid nitrogen temperature (77 K). This simplicity of analysis led to rapid advances in purification (Tannenbaum 1959). The use of highly purified containers of graphite or silica, together with a controlled atmosphere of H_2 which has been passed through a palladium purifier, has led to germanium crystals of a purity unattained by any other elemental substance. Large, highly perfect germanium single crystals can be grown with a total electrically active impurity concentration of less than 10^{10} cm^{-3}, or in chemists' terminology, less than 10^{-7} ppm.

A summary of the major properties of germanium is given in Table I. Extensive data tabulations have been published which attempt a complete survey of the germanium literature (Madelung, 1982, Madelung and Schulz 1987 and 1989).

2. Electronic Properties

2.1. Band structure

The band structure of germanium is shown in Fig. 1. The maximum of the valence band is located at the center of the Brillouin zone while the four conduction band minima are located at the L-points along the four [111] directions. Semiconductors with the maximum of the valence band located at d different value of k than the minimum (minima) of the conduction band are called indirect band gap semiconductors. They are

characterized by long minority carrier lifetimes and very inefficient photon emission upon band-to-band electron-hole recombination.

The valence band edge is derived from the $p_{3/2}$ and $p_{1/2}$ states of the free atom with the $p_{3/2}$ states at the higher energy. The top of the valence band consists of a light and heavy hole band which are degenerate at k=0, the center of the Brillouin zone called Γ point and a third band which is split off by 0.29 eV. The direct and indirect gaps decrease as the temperature is increased as shown in Fig. 2.

2.2. *Impurity and defect levels*

A large number of impurities, defects and their combinations (also called complexes) are known to produce energy levels in the forbidden gap of germanium (Fig. 3). These gap states are conveniently characterized as being donor or acceptor type, shallow (near the corresponding band edges) or deep (far from band edges). As in other semiconductors, there exist single, double and multivalent centers (e.g., double acceptor Be). The energy of the ground states and the excited states of shallow donors (Fig. 4a) and shallow acceptors (Fig. 4b) can be calculated accurately by advanced effective mass theory (Faulkner 1969, Baldereschi and Lipari 1973, 1974).

The shallow levels which are created by the column III and V impurities and lithium have been studied with a wide variety of techniques. In the temperature range where the thermal energy is sufficient to ionize shallow impurities but is too small to create electrons and holes across the bandgap, the free carrier concentration corresponds to the difference of majority and minority dopant concentrations, the so-called net-dopant concentration. The difference is the consequence of the compensation of donors by acceptors and vice versa. Compensation results from the minimum energy principle: an electron of a donor impurity rather occupies an acceptor level which lies much lower in energy than is raised into the conduction band. Variable temperature Hall effect measurements (Yee et al. 1974) give accurate free carrier

concentration values (Fig. 5). The free carrier concentration is an accurate measure of the net-dopant concentration in the temperature range defined above (also called exhaustion or saturation range).

Low temperature optical absorption spectroscopy of lightly doped crystals reveals the hydrogenic bound excited state spectrum of shallow donors and acceptors (Ramdas and Rodriguez, 1980). The development of ultra-pure crystals required a highly sensitive and high resolution characterization technique. Photothermal ionization spectroscopy (PTIS), a two-step ionization process, can generate photoconductivity spectra with line widths of the order of 10 μeV in crystal specimens containing less than 10^6 centers per cm^3. PTIS has led to the discovery of a large number of shallow level centers which contain hydrogen bound to a neutral or a multivalent impurity (Haller et al. 1981, Haller 1986).

The very deep impurities, e.g. the transition metals, have small optical cross-sections and very low solubility and are more conveniently, but less accurately, studied by deep level transient spectroscopy (DLTS) (Pearton 1982) (Fig. 6).

2.3. Electronic transport

2.3.1. Intrinsic conduction. The electrical conductivity is proportional to the product of the number of charge carriers and their mobility. In an intrinsic semiconductor one observes bipolar conduction by electrons and holes. The conductivity is given by:

$$\sigma = n e \mu_e + p e \mu_p \tag{1}$$

where n and p are the electron and hole concentrations and μ_e and μ_p are their respective mobilities. The concentration of charge carriers obeys a mass action law so that at a given temperature $np = n_i^2$ = constant:

$$np = 4\left(2\pi kT/h^2\right)^3 \left(m_e m_h\right)^{3/2} e^{-E_g/kT} \tag{2}$$

where m_e and m_h are the electron and hole effective masses and n_i is the intrinsic carrier concentration. This relation holds over a wide temperature range as is shown experimentally for germanium in Fig. 7. The strong temperature dependence of n_i dominates σ and the weaker power-dependencies of the mobilities do not play a significant role.

2.3.2. Extrinsic conduction. When germanium is doped with shallow donors or acceptors (column III or V elements), n or p becomes much larger than n_i over a wide temperature range and the conductivity will be dominated by the temperature dependence of the mobility. Three major mobility regimes are observed. At high temperatures lattice phonon scattering dominates:

$$\mu_{phonon} \propto T^{-3/2} \tag{3}$$

At lower temperature, ionized impurity scattering limits the mobility:

$$\mu_{ionized\ imp.} \propto \frac{T^{3/2}}{Z^2 N} \tag{4}$$

with Z = number of charges on the ionized impurity and N = concentration of ionized centers. In crystals with very low compensation (several orders of magnitude larger majority than minority dopant concentration) one observes a low temperature regime in which neutral impurity scattering:

$$\mu_{ionized\ imp.} \propto \frac{1}{N} \tag{5}$$

with N = concentration of neutral centers. The total mobility is obtained by adding the inverse mobilities (Matthiessen's rule):

$$\mu_{total} = \left[\frac{1}{\mu_{phonon}} + \frac{1}{\mu_{ionized\ imp.}} + \frac{1}{\mu_{neutral\ imp.}}\right]^{-1} \tag{6}$$

Fig. 8 shows the hole mobilities in two low compensation Ga doped Ge crystals over a wide temperature range. The onset of ionized impurity scattering is clearly seen as an inflection at 60 K. The reason why the mobility continues to rise at lower temperatures lies in the fact that the Ga acceptors freeze out, i.e., they become neutral when they bind a hole at temperatures <20 K. Below ~7 K the mobility becomes constant and is dominated by neutral impurity scattering. In moderately doped crystals which are highly compensated, a large fraction of the acceptors and donors remain ionized and the mobility does not rise because of freezeout. In such material one observes the lattice scattering regime at high temperatures and the ionized impurity scattering regime at low temperatures.

At large impurity concentrations ($>10^{15}$ cm^{-3}) the conductivity is dominated by carrier hopping at low temperatures and at high doping ($>2\times10^{17}$ cm^{-3}), an impurity band forms and the germanium exhibits metallic conduction, (i.e., conduction persists down to T = 0 K). These various conduction regimes are illustrated by experimental data in Fig. 9 for sixteen compensated Ge samples with varying acceptor concentrations. In the most lightly doped sample (#1, $N_A=1.7\times10^{14}$ cm^{-3}) hopping conduction is observed below 5 K and it is rather weak ($\rho \simeq 10^9\ \Omega$ cm). In the extreme of high doping concentration (#15,16) the resistivity stays practically constant at $\sim1.3\times10^{-2}\ \Omega$ cm over the full temperature range. These samples conduct like a metal. The effect of impurity concentration on minority electron mobility in p-type Ge at 300 K is shown in Fig. 10.

The discussion of electrical transport has so far been limited to low electric fields which do not heat up the free carriers to energies larger than kT. At high electric fields the carriers become hot and give up their kinetic energy by generating optical phonons. The carrier drift velocity is observed to saturate at values close to 10^7 cm s^{-1} for electric fields larger than 10^4 V cm^{-1}.

Transport phenomena become very complicated when electric and magnetic fields are present. It has been demonstrated that under appropriate conditions a population inversion of free holes between the light and the heavy hole bands can be achieved with crossed electric and magnetic fields at low temperatures. Such Ge crystals can be induced to lase in the far infrared range of the electromagnetic spectrum (Gornik 1991).

3. Optical Properties

3.1. Linear absorption coefficient and Refractive Index

All semiconductors exhibit a very rich variety of optical properties and Ge is no exception. Pure crystals cooled to low temperatures contain such small concentrations of free carriers that their effects can be ignored. The most striking feature for these conditions is the fundamental absorption edge, the most important feature in a plot of the linear absorption coefficient as a function of photon energy. The absorption edge occurs at an energy corresponding to the minimum band gap (Fig. 11). Because Ge has an indirect band structure, optical transitions of electrons from the top of the valence band at the Γ point of the first Brillouin zone to one of the four conduction band minima at the L-points require assistance of a phonon. This three-particle process is clearly less probable than a direct band gap transition. At photon energies larger > 0.8 eV, direct transitions can occur and the linear absorption coefficient rapidly rises to large values.

The linear absorption coefficient is defined by the following equation:

$$I = I_0 \exp(-\alpha x) \tag{7}$$

I_0 and I are the photon beam intensities before and after passage of the beam through a semiconductor slab of thickness x. The linear absorption coefficient is typically given in units of cm^{-1}. This simple equation does not take into account external or internal reflections caused by a refractive index different from unity.

Below the fundamental absorption edge pure Ge is transparent and is used for a large number of infrared optical components. As a covalently bonded material, Ge is not infrared active, though at low photon energies lattice (multiphonon) absorption gives rise to a broad absorption feature reaching from approximately 25 to 90 meV (ν:200 to 700 cm^{-1}, λ:50 to 14 μm), with α reaching a peak value of 10 cm^{-1} at $h\nu$ = 44 meV (ν=350 cm^{-1}, λ=28.6 μm) at 77 K (Fig. 12).

At even lower photon energies one encounters effects of shallow dopants. The absorption spectrum of a Ge crystal moderately doped with Ga acceptors is shown in Fig. 13. The narrow peaks correspond to hole transitions from acceptor ground states to hydrogenic bound excited states.

For optical applications of Ge it is most useful to discuss the refractive index, n, and the extinction coefficient, k. They are related to the real (ε') and the imaginary part (ε'') of the dielectric constant:

$$\varepsilon = \varepsilon' + i\varepsilon'' \tag{8}$$

$$\varepsilon'(\nu) = n^2(\nu) - k^2(\nu) \tag{9}$$

$$\varepsilon''(\nu) = 2n(\nu)\,k(\nu) \tag{10}$$

The linear absorption coefficient and the wavelength λ are related to k:

$$k = \frac{\alpha\lambda}{4\pi} \tag{11}$$

An extensive tabulation of n and k over a very wide photon energy range can be found in the literature (Potter 1985). A reduced set of values is reproduced in Table II.

3.2. Photoconductivity

In Ge one distinguishes between two classes of optical absorption processes, both leading to an increase in the free carrier concentration. Intrinsic photoconductivity is due to the excitation of an electron across the band gap, while extrinsic photoconductivity is due to the ionization of a neutral donor or acceptor in a cold crystal.

Diode structures are typically used for intrinsic photocarrier generation and collection. Ge photodiodes are widely used for infrared photoluminescence studies. They are sensitive to photons with energies larger than the indirect bandgap (E_{IG}=744 meV). Ge photodiodes are cooled, typically to liquid nitrogen temperature (77 K), in cases where the large dark current caused by room temperature thermal generation interferes with photodetection.

Photons with very large energies such as X-rays and γ-rays produce large numbers of photocarriers per photon. Through the photoeffect the energy of the incoming photons is transferred to a Ge core electron. One electron-hole pair is generated per 3 eV of the energy of the X-ray or γ quantum (Haller and Goulding 1981).

Extrinsic photoconductivity in doped Ge has been applied to far infrared detection. Moderately doped Ge crystals ([Ga] ~ 10^{14} cm^{-3}) with two ohmic contacts are operated in the photoconductor mode. Such devices have to be cooled to liquid helium temperature in order to suppress thermal ionization of the shallow dopants. Typical dopants are Ga, Be and Cu. Extrinsic photoconductors doped with these impurities can detect photons in an energy range from 10 meV (ν=80 cm^{-1}, λ=125 μm) to several hundred meV (ν=1000 cm^{-1}, λ=10 μm) (Haller 1985, Haegel and Haller 1986). Application of uniaxial stress along the [100] axis reduces the hole binding energy to half its unstressed value and shifts the detection limit to 5 meV (40 cm^{-1}, 250 μm) (Hall 1962). Extrinsic Ge photoconductors are the most sensitive photon detectors beyond λ=40 μm. Fig. 14 shows the individually normalized response curves of several extrinsic Ge photoconductors.

A two-step ionization process consisting of excitation of an impurity bound carrier from the ground state to a bound excited state followed by thermal ionization of the excited state to the nearest band was discovered by Lifshits and Nad (1965). The resulting free carriers can be detected with very high sensitivity. This so-called photothermal ionization spectroscopy (PTIS) has been extensively applied to the study

of ultra-pure Ge (Haller 1978, 1986; Haller et al. 1981). It combines high energy resolution with superb sensitivity. In ultra-pure Ge, linewidth as small as 10 μeV have been obtained from hydrogenic spectra of shallow donor complexes D(H,O) and D(Li,O) (Haller et al. 1987, Navarro et al. 1988). Fig. 15 displays the PTIS results obtained with an ultra-pure Ge crystal containing the shallow acceptor complex A(H,C) (Kahn et al. 1987). The four strongest lines are the D and C lines of the acceptors Al and $A(D,C)_2$. Each acceptor has a series of lines. The line spacings between specific pairs of lines are identical for all acceptors because the long range Coulomb potential of the negatively charged acceptor core is the same for all shallow acceptors. The differences in the ground state energies shifts the individual line series to different energies. For ease of identification, the positions of the peaks in each acceptor series has been connected with a horizontal line which is labeled with the acceptor symbol.

3.3. Photoluminescence

Absorption of a photon followed by the emission of a photon is called photoluminescence (PL). The indirect gap band structure of Ge makes PL a rare process because lattice phonon or impurities are required for momentum conservation. The PL photon originates from the decay of a free or bound exciton, an electron and a hole forming a hydrogen-like bound system. A large number of impurity bound excitons have been studied in pure and doped Ge (Skolnik 1989, Thewalt et al. 1987).

A new state of matter, the electron-hole liquid, was predicted (Keldysh 1968) and experimentally verified (Wolfe et al. 1975, Hensel et al. 1977, Jeffries and Keldysh 1983) in pure Ge. This quantum liquid consists of condensed excitons. The electron-hole liquid is unstable because of electron-hole recombination and it has to be regenerated continuously by a laser pumping electrons across the band gap. Fig. 16 shows the PL spectrum of a pure Ge crystal at low temperature optically pumped by a laser. The free exciton peak (FE) corresponds to the band gap energy (744 meV) reduced by the

exciton binding energy of 4 meV and the energy of the phonon (LA) assisting the transition (E_{LA}=27 meV). The electron-hole drop peak (EHD) appears at 709 meV, lower than the FE peak by the EHD binding energy.

Recently, isotopically separated Ge has become available (see Table I). PL studies of such crystals allow the determination of the dependence of the band gap and the phonon energies on isotope mass (Fuchs et al. 1991, Davies et al. 1992). It can be expected that phonon transport and imaging as well as a number of special devices (see Section 6) will benefit from isotopically controlled crystals.

4. Technology

4.1. Production

Germanium concentrates are recovered as a by-product of zinc, copper and lead refining. The concentrates are converted to oxides or germanates and treated with HCl to produce $GeCl_4$. The simple and selective chemistry involved in converting $GeCl_4$ (B.P. 83°C) into high purity germanium contributed to the early success of germanium electronics. To produce polycrystals with less than 1 ppm total impurities, the $GeCl_4$ is distilled in the presence of Cl_2, fractionally distilled in silica vessels, mixed with H_2O to form GeO_2 and finally reduced in H_2 and melted in graphite boats (Bridgers et al. 1958). Any processing scrap, saw dust, etc., can be easily converted to $GeCl_4$ to re-enter the process stream.

4.2. Crystal growth

All electronic applications require germanium in single crystal form and often demand ultra-high purity. Germanium can be purified for certain impurities to better than 10^{-6} ppm by zone refining (Pfann 1966) in silica or graphite boats, a process which was developed originally to produce high purity germanium and now has general

application in the fine chemicals industry. The zone-refined polycrystal is used as a starting charge for single crystal growth.

Single crystal germanium is produced by the Czochralski method (Czochralski 1918, Teal and Little 1950) which has replaced the earlier zone-leveling process (Pfann 1952). In the Czochralski method (CZ) an oriented seed crystal is dipped into a melt and withdrawn with temperature control to produce a cylindrical crystal of the desired diameter. This method produced the first high quality germanium crystals (Bridgers et al. 1958) and is used today for the growth of doped and ultra-pure crystals. The CZ growth of dislocation-free silicon crystals has developed into the large scale industrial production of over 10,000 tons of material per year .

4.3. Impurities and defects

4.3.1. Solubility. The solubility is defined as the maximum concentration of an impurity in a solid phase at a given temperature that can be attained without introducing a phase change. Most impurities in germanium have such low solubilities that they are normally given as atoms cm^{-3} instead of areas in phase diagrams (Fig. 17). As seen in the figure, most of the impurities display retrograde solubility in that the maximum solid solubility occurs below the melting temperature. This phenomenon is illustrated in Fig. 18. The left side of the figure shows the normal case where the maximum solubility occurs at the impurity(A)-germanium(B) eutectic (T_{Eu}), while the right side shows the retrograde case in which the maximum solubility is at a temperature higher than that of the eutectic.

4.3.2. Segregation coefficient. When a solid is in contact with its liquid phase at the melting point, impurities typically will exhibit segregation effects between the two phases which at equilibrium is described by the segregation coefficient, k = impurity concentration in solid/concentration in liquid. The segregation coefficient is related to

several physical properties of the impurity and is shown in Fig. 19 as a function of the heat of sublimation and the maximum solubility C_{max}^{eq} (Fig. 20). Zone purification relies on the phenomenon of impurity segregation in a narrow liquid zone which is heated by a radiofrequency heater coil. Multiple passage along a bar of germanium leads to a redistribution of the impurities along the bar. Impurities with $k<1$ will stay preferably in the liquid and will be carried to one end of the bar while impurities with $k>1$ will accumulate with much less effect on the opposite side. Removal of the impure ends leads to a purified material (Pfann 1966).

4.3.3. Impurity diffusion. The majority of impurities diffuse in germanium by the vacancy mechanism. This mechanism involves diffusion by impurity exchange with vacant lattice sites (vacancies). Since the concentration of vacancies is very small, the diffusion coefficients for impurities moving via vacancy assistance are small (Fig. 21) (Stolwijk 1989). In the very open lattice structure of Ge a number of impurities can occupy interstitial spaces between the host atoms. Li, an interstitial donor, is the prototypical fast interstitial diffusor. Because Li does not form any bonds with the Ge dlattice atoms, little energy (~0.4 eV) is required to jump from one tetrahedral interstitial space to the next. An Arrhenius plot of the diffusion coefficients of several interstitial impurities is given in Fig. 22.

Impurities which have both finite interstitial and substitutional solubilities usually display rapid interstitial diffusion behavior while their electronic properties may be dominated by the substitutional component. Cu is the classical case for this dissociative diffusion mechanism (Stolwijk et al. 1985). In its substitutional position it acts as a triple acceptor as one would expect from its valence of one. In the interstitial form Cu has been characterized as a donor though no energy level has ever been reported.

Impurities in germanium can be divided into groups which have similar properties and are studied by similar techniques. The column III and V impurities are most nearly

germanium-like and thus are the slowest diffusers and have the highest solubility. Being most like the host, the extra or missing valence electron is most weakly bound, has a very large Bohr radius (~100Å) and a consequent large optical cross-section for ionization. These elements always diffuse by the simple vacancy method and are most accurately studied by photo-thermal ionization spectroscopy.

The multivalent donor and acceptor impurities are less Ge-like, diffuse faster and have lower solubilities than the III-V. The multiple charge states of these impurities have been studied by photo absorption and photo conductivity. Diffusion is by the vacancy mechanism.

The transition metals exhibit still lower solubilities and faster diffusion. Their valence electrons are more localized resulting in very small optical ionization cross-sections. These impurities are usually studied by Hall effect or deep level transient spectroscopy. Diffusion occurs via the vacancy mechanism.

A few impurities, e.g., H, Li, Ag, Ni, are fast diffusing interstitial impurities which do not follow the above trends of solubility and ionization energy.

4.3.4. Defects. There exists a rich literature on point and line defects in Ge. Point defects have been generated by various kinds of energetic radiation. Gamma rays and electrons of ~1 MeV are ideally suited to form single point defects. Mashovets (1977) has reviewed the understanding of these vacancy-like defects. The outstanding features of these defects are their strong localization and the resulting depth of the energy levels in the bandgap. Several low temperature annealing stages have been observed. Higher energy radiation produces extended defects which are not understood in detail. It is known though that these defects act as strong trapping and recombination centers and that they compensate shallow dopants turning the crystals high resistivity.

A rich spectrum of dislocations with various Burgers vectors have been studied. The structure of these dislocations closely resembles those found in Si single crystals.

5. Applications

The role of germanium as the dominant semiconductor material for electronic devices such as transistors ended by 1960 and its use has been relegated to those applications where some of its unique properties are of importance. Today's bulk of germanium production is consumed by detectors and optics.

5.1. Photodetectors

The long wavelength cutoff λ_c (in μm) of a semiconductor photodetector is given by

$$\lambda_c = \frac{hc}{E} = \frac{1.24}{E} \tag{12}$$

where E (in eV) is the energy needed to produce a free charge carrier. For a band-to-band transition in room temperature germanium (intrinsic detector) E = 0.66 eV yielding λ_c = 1.8 μm, which includes the technically important 1.3 and 1.5 μm low loss windows in optical fiber communications. Intrinsic germanium photovoltaic detectors are normally reverse biased p-n junctions to minimize both response time (10^{-11} s) and dark current (Sze 1981).

Detectors can also be made using the ionization of impurities to produce charge carriers (extrinsic photodetectors). Group III and V impurities in germanium have ionization energies E_i of about 0.01 eV so that λ_e = 120 μm. Deeper level impurities such as Be, Zn, Hg, Cu and Au can be added to maximize the sensitivity at shorter wavelengths. Also, E_i may be reduced by uniaxial stress along [100] to extend the long wavelength cutoff to 250 μm.

Extrinsic photodetectors must be operated at cryogenic temperatures so that the net-dopants are neutral, i.e., they bind a carrier. These detectors are used as low bias voltage photoconductors to prevent electric field ionization of the impurities (avalanche breakdown) and as a result of this low electric field are much slower than intrinsic p-n

diode detectors. For photoconductors, gain is the ratio of carrier lifetime to carrier transit time so that gain may be traded for speed. In the 30-250 μm wavelength range germanium photoconductors have the highest detectivity of any device (Haller et al. 1979, Haller 1985).

5.2. *Nuclear radiation detectors*

The development of hyper-pure germanium (Hall 1971, Hansen 1971) was driven by a demand for a material to make nuclear radiation detectors (Haller and Goulding 1981). These detectors are giant volume p-i-n diodes (up to 400 cm^3) where the i-region forms the bulk of the device and thin ion implanted p- and n-layers form blocking contacts. The i-layer is lightly doped ($|N_A - N_D| \leq 2\times10^{10}\ cm^{-3}$) and it can be totally depleted at operating bias voltages of a few thousand volts. The relation between the net impurity concentration $|N_A - N_D|$, the bias voltage,V, and the thickness of the region depleted of free carriers, W, is given by:

$$W^2 = \frac{2\varepsilon\varepsilon_0 V}{e(N_A - N_D)}$$

where ε is the dielectric constant, ε_0 is the permittivity of vacuum and e is the charge of the electron. For example, for a depletion layer thickness of 1 cm at 1000 V bias, $|N_A - N_D|$ must be less than $2\times10^{10}\ cm^{-3}$.

These detectors are used as single particle or photon energy spectrometers. On average, 3 eV of incident energy are required to produce one electron-hole pair. The ultimate energy resolution is dominated by the statistical nature of the charge production processes. Because these processes are not independent they do not follow normal statistics. The fluctuation in the number of electron-hole pairs ΔN is given by:

$$\Delta N = (FN)^{1/2}$$

with F=0.08 (Fano factor). The full width of a 1 MeV gamma ray peak at half maximum (FWHM) can be as small as 1.2 keV, a factor of 30 smaller than a line produced by a scintillation detector. That the fluctuation in the number of electron-hole pairs is smaller

than the standards statistical fluctuation is related to the fact that the ionization events are not completely random and unrelated.

5.3. Low temperature Ge thermistors

Strong interest in reliable and reproducible temperature sensors by the astrophysical, radio astronomy and "dark matter" search communities in the sub 1 K range has led to a strong development effort of neutron transmutation doped (NTD) Ge material and devices. NTD offers the most homogeneous and controlled doping technique (Larrabee 1984). NTD Ge is unique among semiconductors because it contains both acceptors (Ga) and donors (As) in a fixed ratio given by the natural abundance of ^{70}Ge and ^{74}Ge and their thermal neutron capture cross sections (Haller et al. 1984). NTD Ge can be produced with resistivities ranging from 1 Ω cm to 10^9 Ω cm in a temperature range from 1 K to 15 m K. The NTD Ge thermistors are heat sensitive and do not exhibit any specific wavelength cut off limits. The typical device has submillimeter dimensions to decrease thermal mass and is equipped with two boron ion implanted, degenerately doped p-contacts (Haller 1985).

Non-linear conduction phenomena at very low temperature have led to interesting transport studies (Kenny 1989, Wang 1990).

5.4. Optics

The consumption of germanium for infrared optics now exceeds all other uses combined. The attraction of germanium for this application is its environmental inertness, good mechanical properties, moderate cost, very low dispersion and transparency from 2 to 15 μm. Germanium's only drawback has been its high refractive index (4.0) and the difficulty of making tough anti-reflection coatings. This anti-reflection problem has now been solved by an ideal coating, diamond-like carbon, which is super-tough and has a refractive index of 2.0.

Germanium exhibits significant absorption of infrared radiation in the 15 to 40 μm range due to intrinsic crystal lattice phonon resonances (Fig. 12). Unless specially purified, germanium will also show an absorption line at 11.7 μm due to the local vibrational mode of oxygen impurities.

5.5. *Miscellaneous uses*

Graded index optical fibers are made using a high index of refraction germanium doped silicon core. Germanium has an almost perfect lattice match to GaAs so that high quality epitaxial layers can be grown. These Ge-GaAs bilayers have produced the highest efficiency solar cells. Impatt diodes, tunnel diodes (Sze 1981) and phonon drag detectors are made from germanium. A population inversion in the heavy hole-light hole bands can be induced in p-type germanium in crossed electric and magnetic fields at low temperature to produce a tunable, long wavelength laser (Gornik 1991).

A research area of great current interest is the prospect of integrating quantum well structures on silicon using germanium. Considerable progress has been made in producing Ge-Si strained layer superlattices for photodetectors and transistors (Bean et al. 1991).

Glossary

Diamond lattice: The diamond lattice structure consists of a regular array of points in space. The corners and the centers of each face of two intersecting cubes describe the basic building block of the diamond lattice. Putting real atoms on all of these lattice points leads to a crystal. These atoms form covalent bonds with each of the four nearest neighbors. Carbon, silicon and germanium crystallize in the diamond structure.

Band structure: Electrons in solids can only assume energies in certain ranges called allowed bands. Forbidden energy ranges are called band gaps. Depending on the degree to which the highest allowed energy band is filled with electrons, and depending on the width of the band gap, a solid is an electrical conductor, an insulator, or a semiconductor.

Brillouin Zone: The regular spacing of atoms in a crystal lattice can be represented by points in an inverse or reciprocal space, also called momentum space. The Brillouin zone occupies part of this space. Every point on the Brillouin zone surface is the end point of a factor signifying a diffraction condition of the real space crystal lattice.

Valence band: The highest energy band filled with electrons. Missing electrons in the band, holes, can conduct electricity in the valence band.

Conduction band: The first allowed energy band above the band gap in semiconductors or insulators. Electrons in this band are free to move and conduct electricity.

Bound excited state: Electrons (holes) are bound to a donor (acceptor) by the Coulomb field of the positive (negative) charge at the donor

(acceptor) core. As in a hydrogen atom there exists a ladder of discrete energy states in which the electron (hole) can exist. The lowest energy state is the ground state, all other states below the conduction band edge (above the valence band edge) are bound excited states. Because of the strong analogy between donors (acceptors) and the hydrogen atom, bound excited states are often called hydrogenic states or hydrogenic bound excited states.

Hydrogenic states: Bound excited states.

Holes: See valence band.

Effective mass: The Newtonian principle equating force with the product of mass and acceleration can be transferred to electrons (holes) in a semiconductor crystal. Because of the wave nature of electrons (holes), motion in a crystal with regular atom spacings is altered and an effective mass different from the free electron mass is introduced to describe the motion of electrons (holes). The curvature of the conduction band minimum (valence band maximum), i.e., the second derivative of these curves (see Fig. 1) are inversely proportional to the effective mass.

Photothermal ionization spectroscopy (PTIS): Excitation of an electron (hole) at low temperatures from the ground state to one of the bound excited states in a donor (acceptor) can be followed by further excitation through thermal energy (a phonon) into the conduction (valence) band. The resulting free carrier will change the electrical conductivity of the crystal. The intense conductivity peaks at photon energies corresponding precisely to ground state to bound excited state transitions have become the most sensitive and precise

tool in the study of impurities and defects in numerous semiconductor crystals.

Vacancy: A crystal lattice site without an atom occupying it. Vacancies play a very important role in the motion of impurities and defects through a crystal.

Interstitial: An impurity or host atom located off a lattice site. Interstitials can be very mobile in the wide open diamond lattice and play an important role in impurity and defect motion (see vacancy).

Fano factor: The factor by which the statistical fluctuations in the production of electrons and ions in a gas or electrons and holes in a semiconductor deviate from normal statistics.

Neutron transmutation doping (NTD): The exposure of a semiconductor to thermal neutrons in a nuclear reactor leads to the formation of neutron-rich nuclei through neutron capture. Such nuclei are often unstable and decay into nuclei of a different element. Most often used for silicon, NTD produces phosphorus donors in this semiconductor. In Ge both Ga acceptors and As donors are formed through NTD.

List of Works Cited

Baldereschi A and Lipari N O, 1973, Phys. Rev. B 8, 2697-2709; 1974 Ibid. 9, 1525-1539; Proceedings XIII International Conference on the Physics of Semiconductors, Rome, Fumi, (Ed.), North Holland, Amsterdam, p. 595-598.

Bardeen J and Brattain W, 1948, Phys. Rev. 74, 230-231.

Bean J C, Iyer S S, and Wang K L, 1991, Silicon Molecular Beam Epitaxy, Proc. Mat. Res. Soc. Vol. 220, Materials Research Society, Pittsburg, PA.

Biondi, F J, 1958, Transistor Technology, Vols. II and III, D. Van Nostrand Co. Inc., Princeton, New Jersey.

Bridgers H E, Scaff J H, Shive J N (Eds.) 1958, Transistor Technology, Vol. I, Van Nostrand Co. Inc., Princeton, New Jersey.

Collins R J and Fan H Y, 1954, Phys. Rev. 93, 674-678.

Czochralski J, 1918, Zeitschrift für Physik 92, 219-221.

Davis G, Lightowlers E C, Ozhogin V, Itoh K, Hansen W L, and Haller E E, 1992, Proc. 5th Intl. Conf. on Shallow Impurities in Semiconductors, Kobe, in press.

Faulkner R A, 1969, Phys. Rev. 184, 713-721.

Fishler S, 1962, J. Appl. Phys. 33, 1615.

Frank W, Gösele V, Mehrer H and Seeger A, 1984, in Diffusion in Crystalline Solids, Murch GE and Norwick AS, (Eds.) Academic Press, pp. 63-142.

Fritzsche H and Cuevas M, 1960, Phys. Rev. 119, 1238-1245.

Fuchs H D, Grein C H, Thomson C, Cardona M, Hansen W L, Itoh K, and Haller E E, 1991, Phys. Rev. B 43, 4835-4842.

Gornik E, 1991, Optical and Quantum Electronics 23, No. 2, Special Issue on Far-infrared Semiconductor Lasers.

Hall J J, 1962, Phys. Rev. 128, 68-75.

Hall R N and Soltys T J, 1971, IEEE Trans. Nucl. Sci. 18, 160-169.

Haller E E, 1978, Phys. Rev. Lett. 40, 584-586.

Haller E E, 1985, Infrared Physics 25, 257-266.

Haller E E, 1986, in Adv. in Sol. State Phys. XXVI, Grosse P (Ed.), Vieweg, p. 203-229.

Haller E E, Hueschen M R, and Richards P L, 1979, Appl. Phys. Lett. 34, 495-497.

Haller E E and Falicov L M, 1978, Phys. Rev. Lett. 41, 1192-1194.

Haller E E and Goulding F S, 1981, Handbook on Semiconductors Vol. 4, Chapter 6C, Hilsum C (Ed.), North-Holland, Amsterdam, p. 799-827.

Haller E E, Hansen W L and Goulding F S, 1981, Adv. in Physics 30, 93-138.

Haller E E, Palaio N P, Rodder M, Hansen W L, and Kreysa E, 1984, Proc. Fourth Intl. Confr. on Neutron Transmutation Doping of Semiconductor Materials, Larrabee R D (Ed.), Plenum Press, p. 21-36.

Hansen W L, 1971, Nucl. Instr. & Meth. 94, 377-380.

Hensel J C, Thomas G A, Phillips T G, and Rice T M, 1977, Solid State Physics Vol. 32, Ehrenreich H, Seitz F, and Turnbull D (Eds.), Academic Press, NY.

Hueschen M, 1981, private communication.

Jeffries C D and Keldysh L V, 1983, Electron Hole Droplets in Semiconductors, Modern Problems in Cond. Matter Series, Vol. 6, Agronovich V M and Meradudin A A (Eds.), North-Holland, Amsterdam.

Jones R L and Fisher P, 1965, J. Phys. Chem. Solids 26, 1125-1131.

Kahn J M, McMurray Jr. R E, Haller E E, and Falicov L M, 1987, Phys. Rev. B 36, 8001-8014.

Keldysh L V, 1968, Proc. 9th Intl. Confr. Physics of Semiconductors, Moscow, Nauka, Leningrad, p. 1303-1312.

Kelso S, 1979, PhD thesis, Physics Dept. University of California at Berkeley and Lawrence Berkeley Laboratory, Report LBL-8786.

Kenny T W, Richards P L, Park I S, Haller E E and Beeman J, 1989, Phys. Rev. B 39, 8476-8482.

Kittel C, 1986, Introduction to Solid State Physics, 6th edition, Wiley, New York, p. 199.

Larrabee R D (Ed.) 1984, Proc. Fourth Intl. Confr. on Neutron Transmutation Doping of Semiconductor Materials, Plenum Press.

Lifshits T M and Nad F Ya, 1965, Sov. Phys. Dokl. 10, 532-533.

Madelung O (Ed.) 1982, Semiconductors: Physics of Group IV Elements and III-V Compounds, Landolt-Börnstein, Series III, Vol. 17a, Springer, Berlin.

Madelung O and Schulz M (Eds.) 1987, Semiconductors: Intrinsic Properties of Group IV Elements and III-V, II-VI and I-VII Compounds, Landolt-Börnstein, Series III, Vol. 22a, Springer, Berlin.

Madelung O and Schulz M (Eds.) 1989, Semiconductors: Impurities and Defects in Group IV Elements and III-V Compounds, Landolt-Börnstein, Series III, Vol. 22b, Springer, Berlin.

Mashovets T V, 1977, Inst. Phys. Confr. Series 31, 30-44.

McLean T P, 1960, Progress in Semiconductors, Vol. 5, Gibson A F (Ed.), Heywood, London.

Morin F J and Maita J P, 1954, Phys. Rev. 94, 1525-1529.

Navarro H, Haller E E, and Keilmann I, 1988, Phys. Rev. B 37, 10822-10828.

Pearton S J, 1982, Solid State Electronics 25, 499-503.

Pfann W G, 1952, Trans. of the A.I.M.E. 194, 747-753.

Pfann W G, 1966, Zone Melting, Wiley, New York.

Potter R F, 1985, in Handbook of Optical Constants of Solids, Palik E D (Ed.), Academic Press, New York, pp. 465-478.

Prince M B, 1953, Phys. Rev. 92, 681-687.

Ramdas A K and Rodriguez S, 1981, Rep. Prog. Physics 44, 1297-1387.

Rhodes R G, 1964, Imperfections and Active Centers in Semiconductors, Pergamon Press, p. 213.

Shockley W, 1949, Bell Sys. Tech. J. 28, 435-489.

Shockley W and Pearson G, 1948, Phys. Rev. 74, 232-233.

Skolnick M S, 1989, Landolt-Börnstein, Series III, Vol. 22b, Springer, Berlin, p. 466-489.

Stolwijk N A, 1989, Landolt-Börnstein, Series III, Vol. 22b, Springer, Berlin, p. 439-465,

Stolwijk N A, Frank W, Hölzl J, Pearton S J, and Haller E E, 1985, J. Appl. Phys. 57, 5211-5219.

Sze S M, 1981, Physics of Semiconductor Devices, second edition, Wiley, New York.

Tannenbaum M, 1959, in Semiconductors, Hannay B, (Ed.), Reinhold, p. 87.

Teal G K and Little J B, 1950, Phys. Rev. 78, 647.

Thewalt M L W, Labrie D, Booth I J, Clayman B P, Lightowlers E C, and Haller E E, 1987, Physica 146B, 47-64.

Torrey H C and Whitmar C A, 1948, Crystal Rectifiers, MIT Rad. Lab. Series Vol. 15, McGraw-Hill, New York.

Trumbore F A, 1960, Bell Sys. Tech. J. 39, 205-234.

Wang N, Wellstood F C, Sadoulet B, Haller E E, and Beeman J, 1990, Phys. Rev. B 41, 3761-3768.

Weber E R, 1983, Appl. Phys. A 30, 1-22.

Winkler C, 1886, J. für Praktische Chemie, Neue Folge 34, 177-229.

Wolfe J P, Hansen W L, Haller E E, Markiewicz R S, Kittel C, and Jeffries C D, 1975, Phys. Rev. Lett. 34, 1292-1293.

Yee J H, Swierkowski S P, Armantrout G A, and Wichner R, 1974, J. Appl. Phys. 45, 3949-3954.

Table I.

Properties of germanium.

Property	Value
Atomic number	32
Atomic weight	72.59
Natural isotopic composition (%)	
70	20.4
72	27.4
73	7.8
74	36.6
76	7.8
Density (25°C, g cm^{-3})	5.3234
Atomic density (atoms cm^{-3})	4.416×10^{22}
Crystal structure	diamond cubic
Lattice parameter at 300 K (Å)	5.64613
Melting point (mp) (°C)	937.4
Boiling point (°C)	2830
Vapor pressure at mp (atm)	2×10^{-13}
Volume contraction on melting (%)	4.7
Heat of fusion (kJ mol^{-1})	36.945
Heat of sublimation (kJ mol^{-1})	374.5
Thermal expansion coefficient at 300 K (10^{-6} K^{-1})	5.9
Thermal conductivity at 300 K (W cm^{-1} K^{-1})	0.6
Energy gap at 300 K (eV)	0.664
Energy gap at 0 K (eV)	0.744

Elastic stiffness constants at 25°C (10^{11} dyn/cm^2)	C_{11}	12.40
	C_{12}	4.13
	C_{44}	6.83
Intrinsic resistivity at 25°C (Ω cm)		50
Intrinsic electron concentration at 300 K (cm^{-3})		1.38×10^{13}
Temperature dependence of intrinsic concentration (cm^{-3})		$1.76\times10^{16}\ T^{3/2} \exp(-0.785/2kT)$
Intrinsic electron mobility at 300 K (cm^2 V^{-1} s^{-1})		3900
Intrinsic hole mobility at 300 K (cm^2 V^{-1} s^{-1})		1800
Effective mass, m/m_0		
electrons;	longitudinal	1.64
	transverse	0.082
holes;	light	0.044
	heavy	0.28
Refractive index, 2.5–150 μm		4.0
Dielectric constant		16.0

Table II.

Refractive Index and Extinction Coefficient k as a function of photon energy E. (after Potter 1985)

E (eV)	n	k
525.3	0.99741	9.8×10^{-4}
100	–	2.57×10^{-2}
50	–	4.52×10^{-2}
10	0.93	0.86
5	1.394	3.197
4	3.905	3.336
3	4.082	2.145
2	5.588	0.933
1	4.325	8.09×10^{-2}
0.8	4.275	5.67×10^{-3}
0.66	–	6.73×10^{-5}
0.60	–	6.58×10^{-7}
0.59	4.104	–
0.20	4.011	–
0.099	4.003	–
0.062	3.999	3.98×10^{-4}
0.031	3.983	8.5×10^{-4}
0.0099	4.007	–
0.0025	4.004	4.77×10^{-3}

Figure Captions

Fig. 1 Band structure of germanium. The low temperature indirect gap is 0.744 eV and the direct bandgap is 0.898 eV. (after Kittel 1986)

Fig. 2 Indirect (E_{IG}) and (E_{DG}) energy gaps vs. temperature. (after McLean 1960)

Fig. 3 Impurity energy levels in the forbidden gap of germanium. (after Sze 1981)

Fig. 4a Energy levels of shallow donors with the theoretical and experimental $2P_{\pm}$ levels aligned. (after Faulkner 1969)

Fig. 4b Energy levels of shallow acceptors with experimental and theoretical levels aligned for the $2\Gamma_8$ levels. (after Baldereschi and Lipari 1973,1974)

Fig. 5 Free hole concentration in an ultra-pure Ge sample as measured by Hall effect. (after Yee et al. 1974)

Fig. 6 Detrapping time constants of deep level impurities thermally diffused into germanium, measured by deep level transient spectroscopy. (after Pearton 1982)

Fig. 7 The conductivity of intrinsic Ge vs. temperature. (after Morin and Maita 1954)

Fig. 8 Hall mobility in two moderately doped Ge:Ga crystals. (after Hueschen 1981)

Fig. 9 Resistivity of p-type germanium with compensation K ($=N_D/N_A$)=0.4 (after Fritzsche and Cuevas 1960). The concentrations of acceptors are as follows (in cm^{-3}): (1) 7.5×10^{14}; (2) 1.4×10^{15}; (3) 1.5×10^{15}; (4) 2.7×10^{15}; (5) 3.6×10^{15}; (6) 4.9×10^{15}; (7) 7.2×10^{15}; (8) 9.0×10^{15}; (9) 1.4×10^{16}; (10) 2.4×10^{16}; (11) 3.5×10^{16}; (12) 7.3×10^{16}; (13) 1.0×10^{17}; (14) 1.5×10^{17}; (15) 8.8×10^{17}; (16) 1.35×10^{18}.

Fig. 10 Drift mobility of minority electrons in p-type Ge at 300 K as a function of acceptor concentration. The solid line is calculated. (after Prince 1953)

Fig. 11 Linear absorption coefficient of Ge near the fundamental absorption edge vs. photon energy at 77 K and 300 K.

Fig. 12 Optical absorption coefficient, α, in the far infrared as a function of photon wave-number. (after Collins and Fan 1954)

Fig. 13 The absorption spectrum of Ge doped with 2×10^{14} cm^{-3} Ga. (after Jones and Fisher 1965)

Fig. 14 Responsivity of extrinsic Ge photoconductors doped with various impurities (Haller 1985)

Fig 15 Photothermal ionization line spectrum of the shallow deuterium-carbon acceptor complex A(D,C) of Al and of traces of B. The fact that two line series A(D,C), and $A(D,C)_2$ belong to one acceptor is most unusual and is due to a splitting in the ground state of this acceptor complex. The sample contains approximately 10^9 acceptors. (after Kahn et al. 1987)

Fig. 16 Photoluminescence spectrum of optically pumped pure Ge at low temperature. The free exciton (LA assisted) and electron-hole drop peaks are clearly visible. (after Kelso 1979)

Fig. 17 Solid solubility of impurities in germanium illustrating retrograde solubility. (after Trumbore 1960)

Fig. 18 Phase diagram illustrating the phenomena of retrograde solubility (right hand side). The left side of the figure illustrates the usual case with the maximum solubility at the eutectic temperature. (after Weber 1983)

Fig. 19 Segregation coefficient of impurities vs. heat of sublimation. (after Trumbore 1960)

Fig. 20 Segregation coefficient k_m^{eq} vs. maximum solubility C_{max}^{eq} for impurities in germanium. (after Fishler 1962)

Fig. 21 Diffusion coefficient of impurities which diffuse by the vacancy mechanism. These are all slowly or moderately migrating elements. (after Stolwijk 1989)

Fig. 22 Diffusion coefficient of impurities which diffuse by the interstitial mechanism. These are all fast migrating elements. (after Stolwijk 1989)

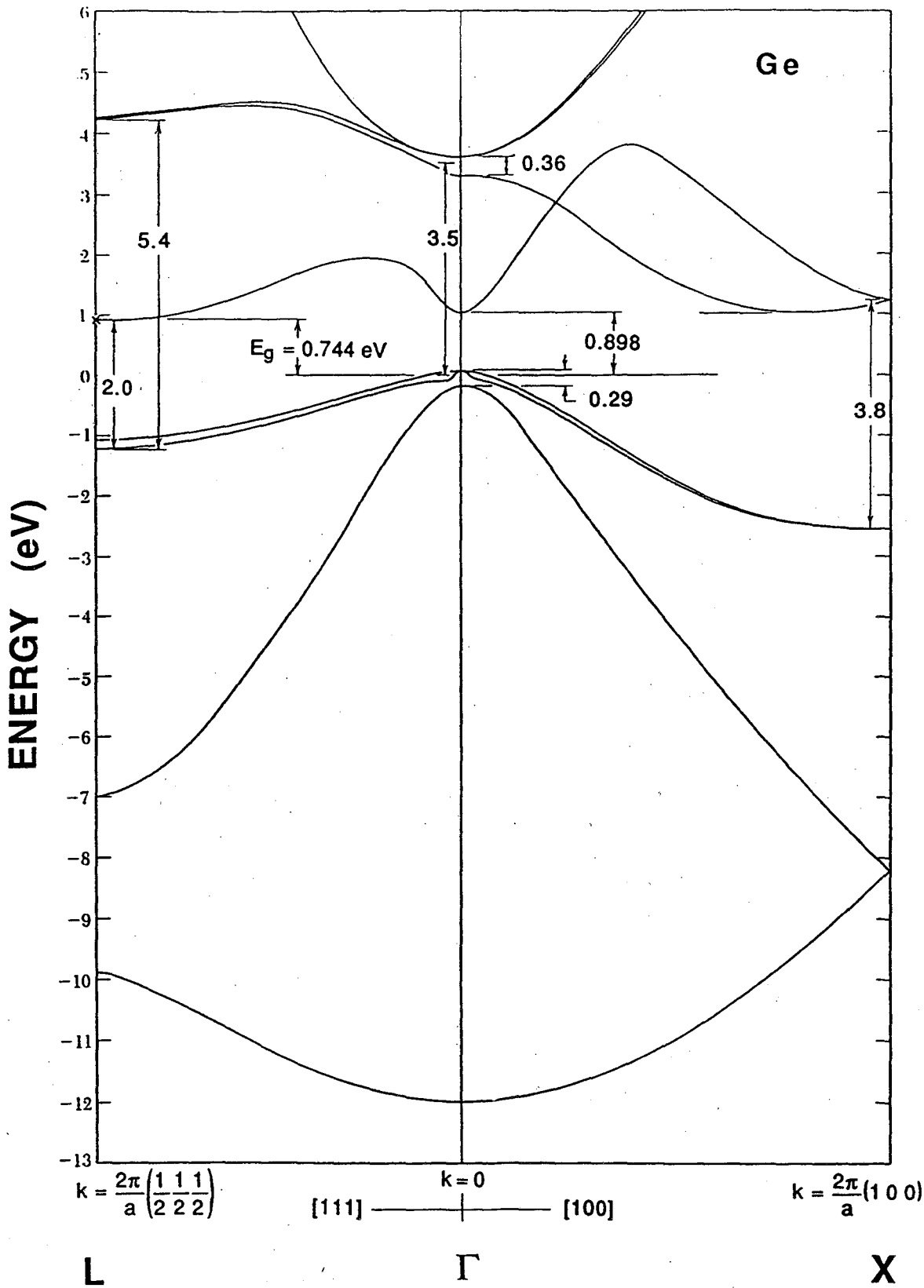
Ge
ENERGY (eV)
6
5
4
3
2
1
0
−1
−2
−3
−4
−5
−6
−7
−8
−9
−10
−11
−12
−13
5.4
3.5
0.36
2.0
E_g = 0.744 eV
0.898
0.29
3.8
k = 2π/a (1/2 1/2 1/2)
k = 0
[111]
[100]
k = 2π/a (1 0 0)
L
Γ
X

Figure 1

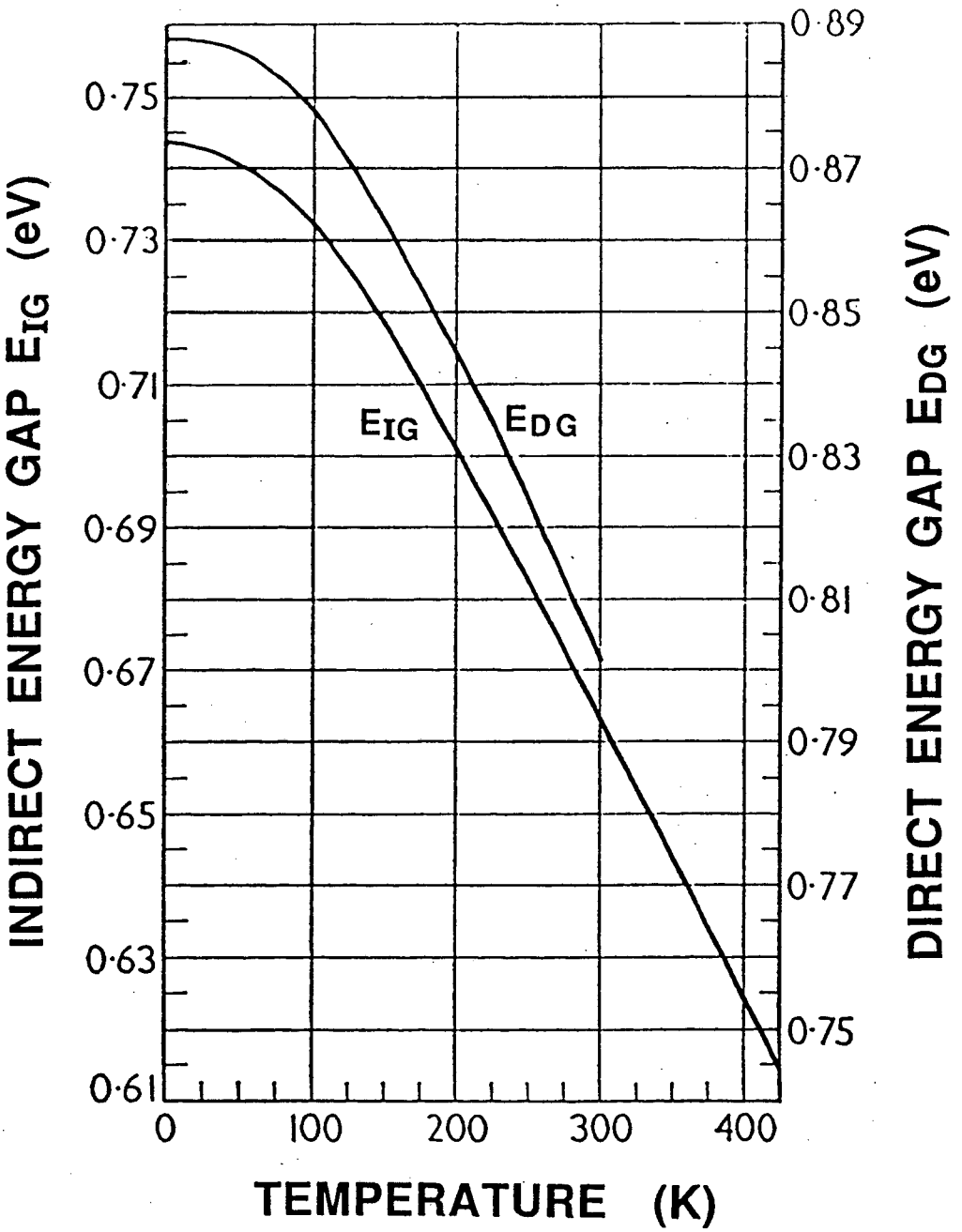
INDIRECT ENERGY GAP E_{IG} (eV)
0·75
0·73
0·71
0·69
0·67
0·65
0·63
0·61
0
100
200
300
400
TEMPERATURE (K)
E_{IG}
E_{DG}
0·89
0·87
0·85
0·83
0·81
0·79
0·77
0·75
DIRECT ENERGY GAP E_{DG} (eV)

Figure 2

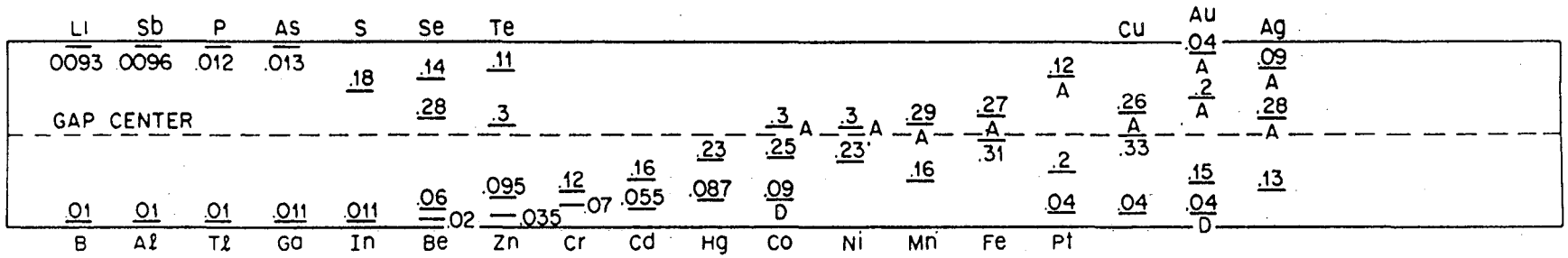

IMPURITY SPECIES

FIG

Figure 3

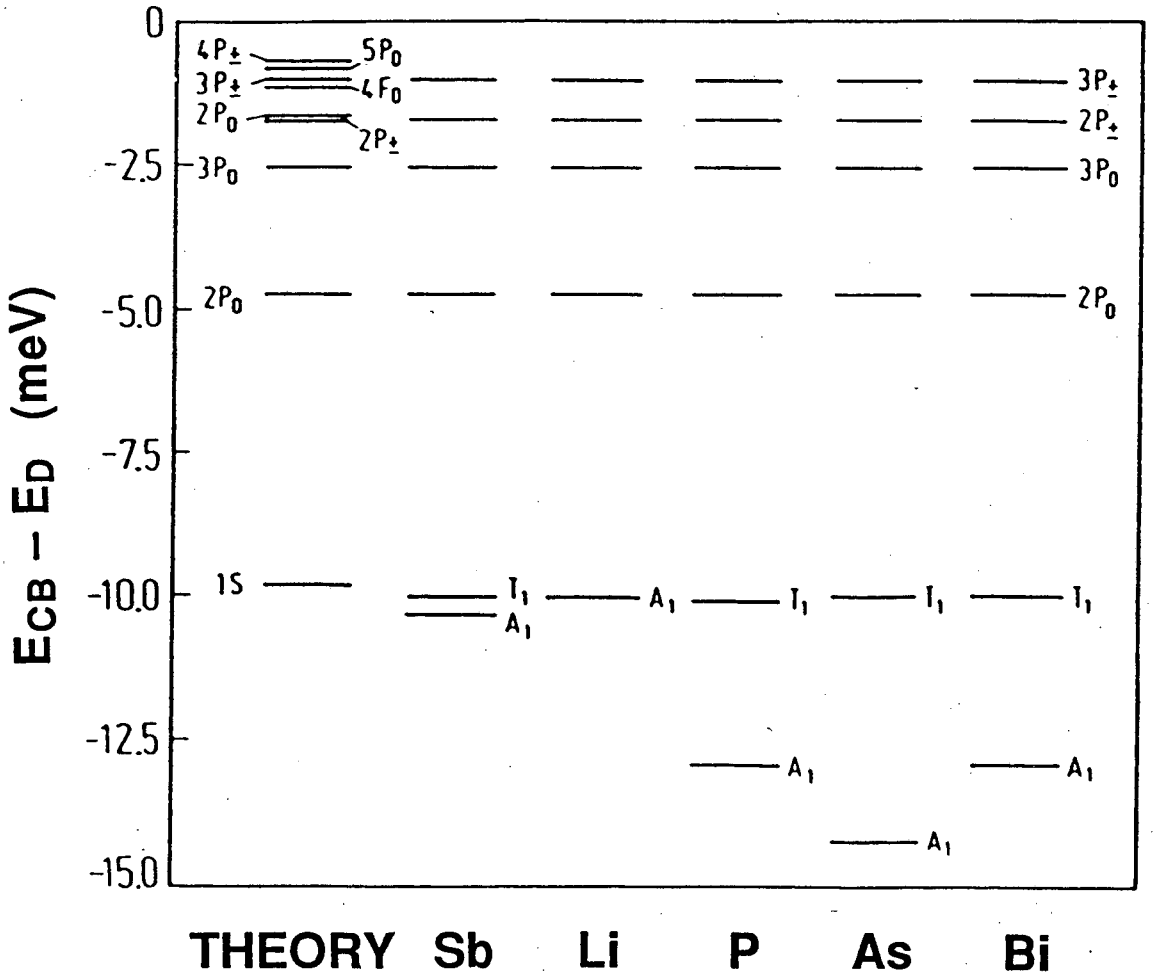
0
-2.5
-5.0
-7.5
-10.0
-12.5
-15.0
$E_{CB} - E_D$ (meV)
$4P_\pm$
$3P_\pm$
$2P_0$
$5P_0$
$4F_0$
$2P_\pm$
$3P_0$
$2P_0$
1S
T_1
A_1
A_1
T_1
A_1
A_1
T_1
A_1
A_1
T_1
$3P_\pm$
$2P_\pm$
$3P_0$
$2P_0$
A_1
THEORY
Sb
Li
P
As
Bi

Figure 4a

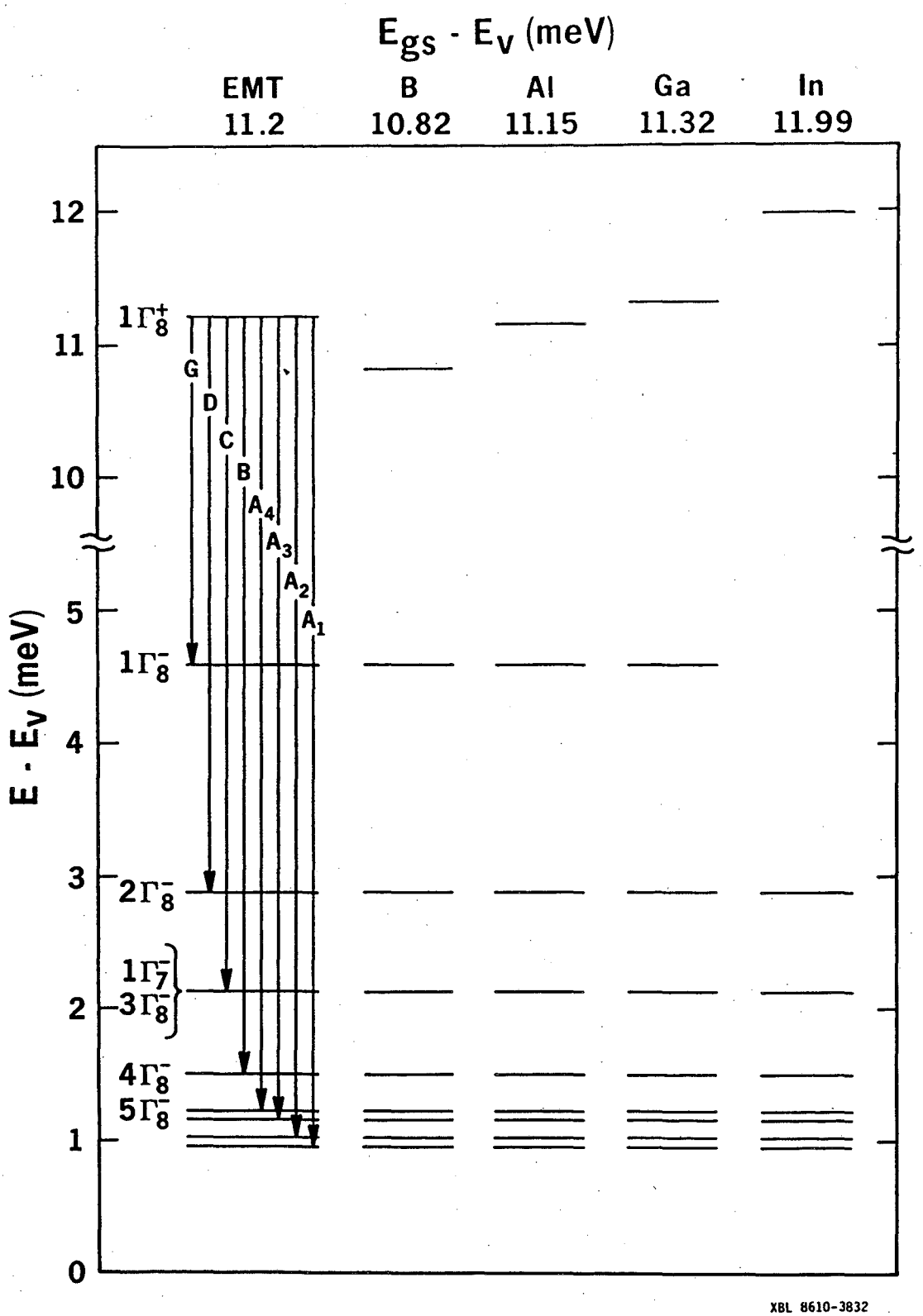
$E_{gs} - E_v$ (meV)
EMT
11.2
B
10.82
Al
11.15
Ga
11.32
In
11.99
$E - E_v$ (meV)
12
11
10
5
4
3
2
1
0
$1\Gamma_8^+$
$1\Gamma_8^-$
$2\Gamma_8^-$
$1\Gamma_7^-$
$3\Gamma_8^-$
$4\Gamma_8^-$
$5\Gamma_8^-$
G
D
C
B
A_4
A_3
A_2
A_1
XBL 8610-3832

Figure 4b

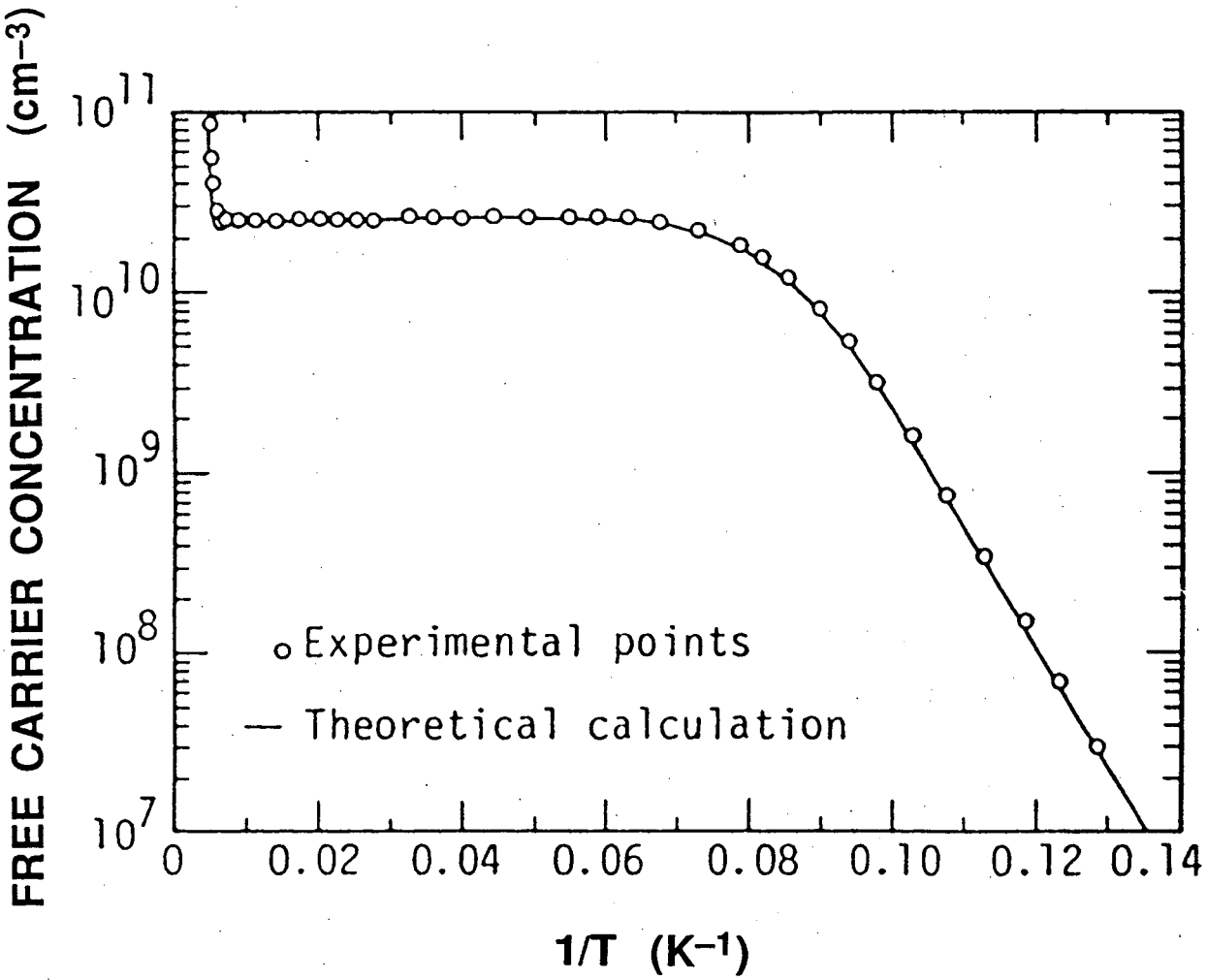
FREE CARRIER CONCENTRATION (cm-3)
10^11
10^10
10^9
10^8
10^7
0
0.02
0.04
0.06
0.08
0.10
0.12
0.14
1/T (K-1)
o Experimental points
— Theoretical calculation

Figure 5

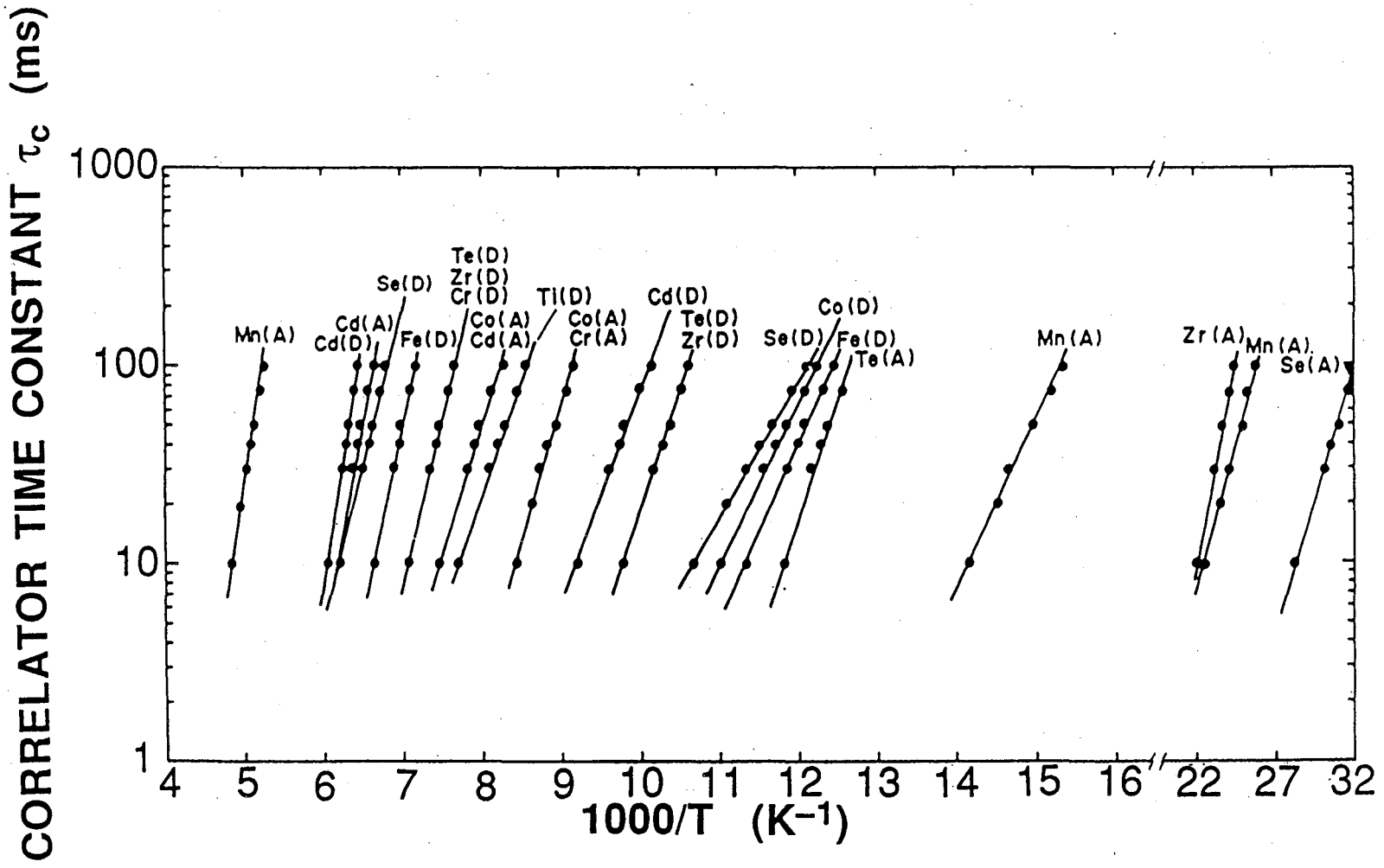
CORRELATOR TIME CONSTANT τ_c (ms)
1000
100
10
1
4
5
6
7
8
9
10
11
12
13
14
15
16
22
27
32
1000/T (K^{-1})
Mn(A)
Cd(A)
Cd(D)
Se(D)
Fe(D)
Te(D)
Zr(D)
Cr(D)
Co(A)
Cd(A)
Tl(D)
Co(A)
Cr(A)
Cd(D)
Te(D)
Zr(D)
Co(D)
Se(D)
Fe(D)
Te(A)
Mn(A)
Zr(A)
Mn(A)
Se(A)

Figure 6

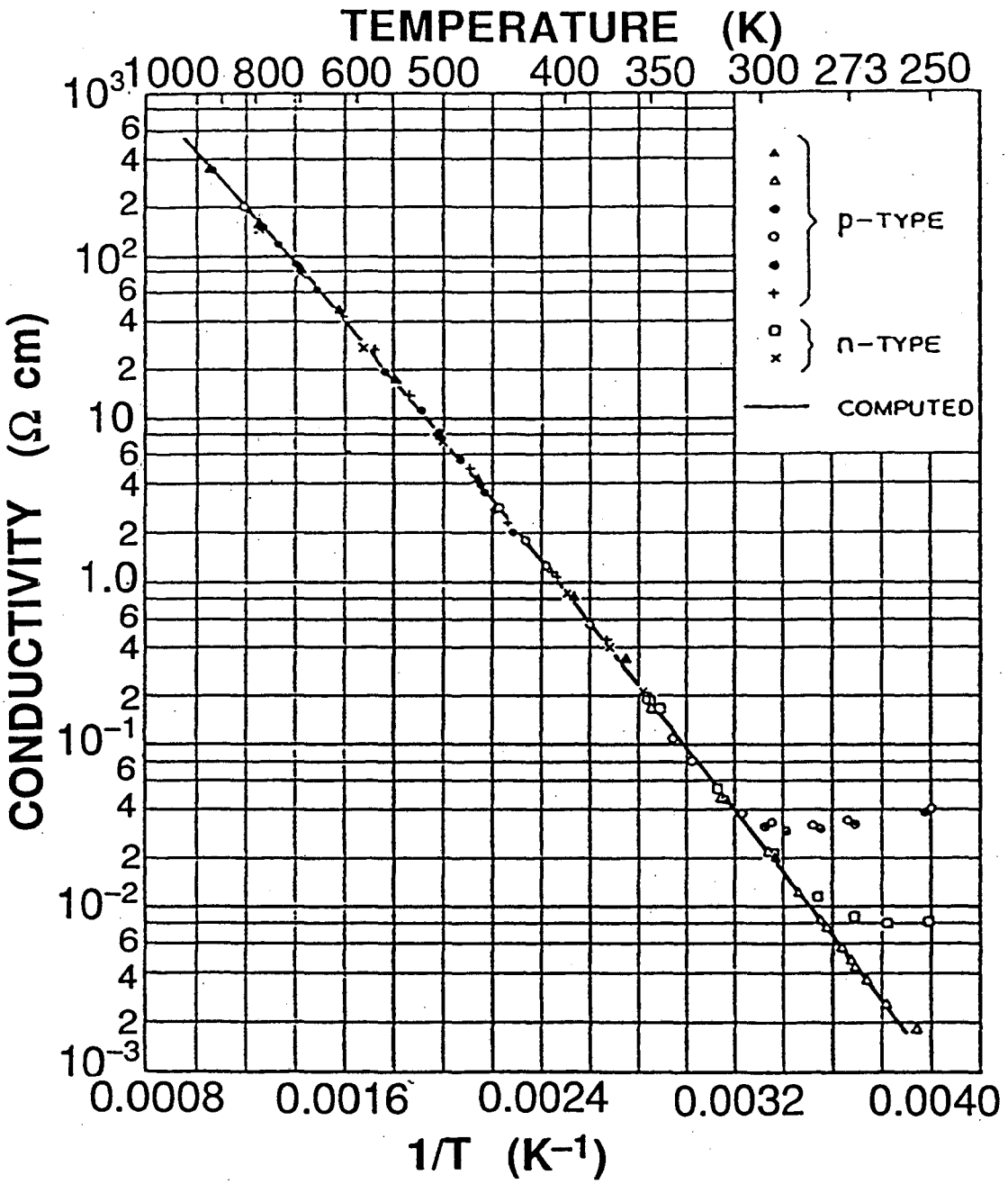
TEMPERATURE (K)
1000 800 600 500 400 350 300 273 250
CONDUCTIVITY (Ω cm)
10³
10²
10
1.0
10⁻¹
10⁻²
10⁻³
0.0008 0.0016 0.0024 0.0032 0.0040
1/T (K⁻¹)
p-TYPE
n-TYPE
COMPUTED

Figure 7

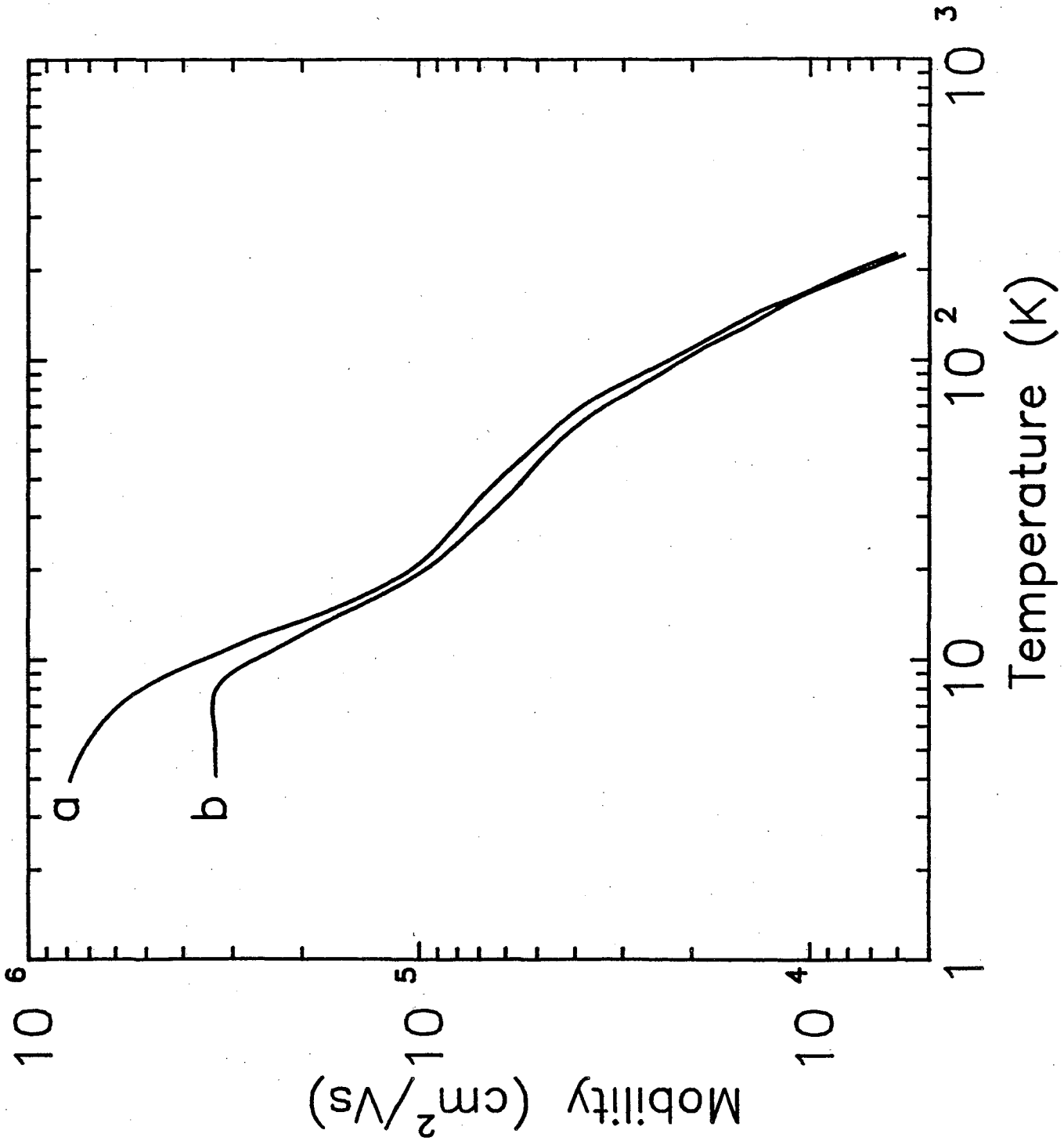

Figure 8

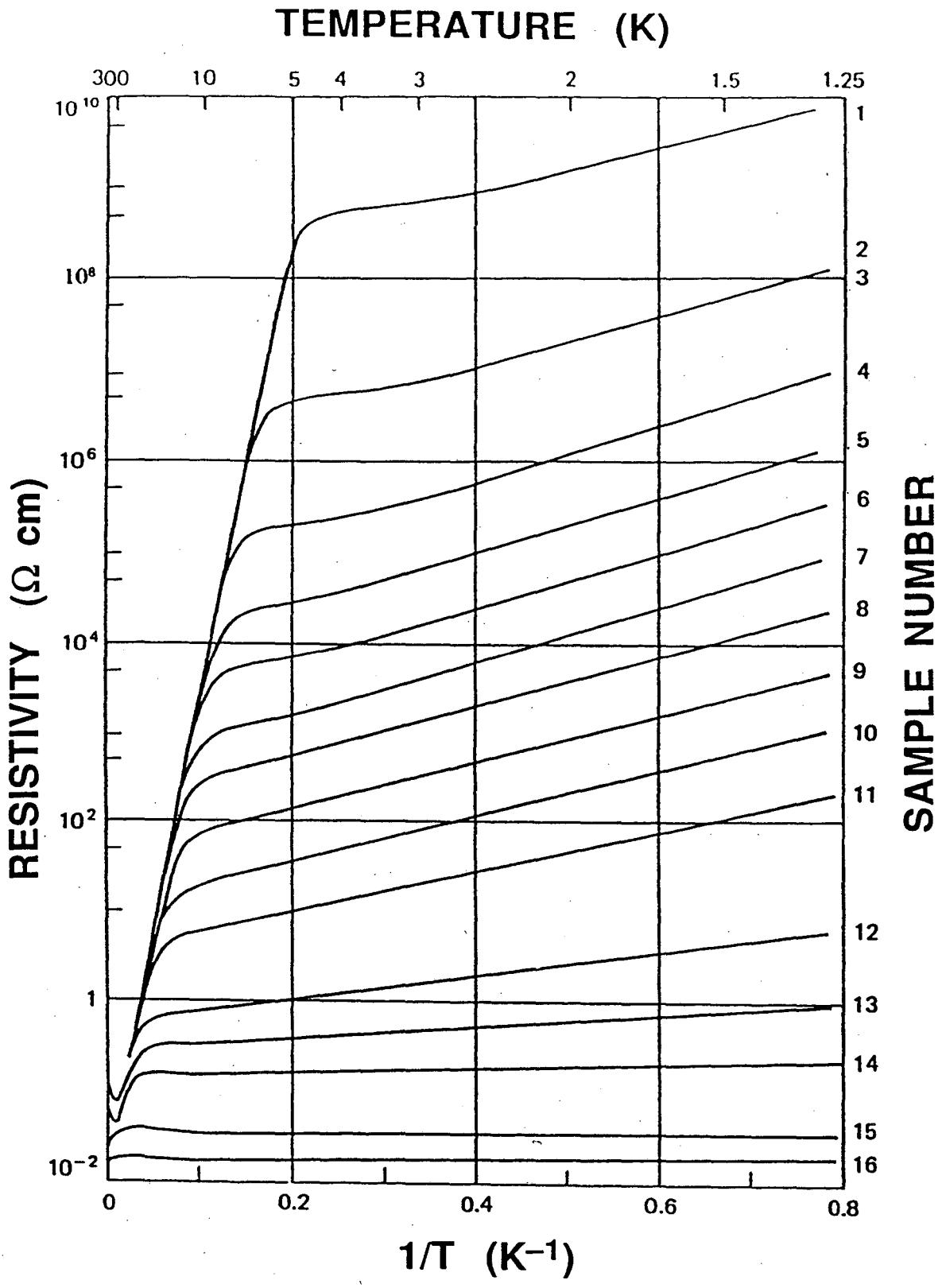
TEMPERATURE (K)
300
10
5
4
3
2
1.5
1.25
10^{10}
10^8
10^6
10^4
10^2
1
10^{-2}
RESISTIVITY (Ω cm)
1
2
3
4
5
6
7
8
9
10
11
12
13
14
15
16
SAMPLE NUMBER
0
0.2
0.4
0.6
0.8
1/T (K^{-1})

Figure 9

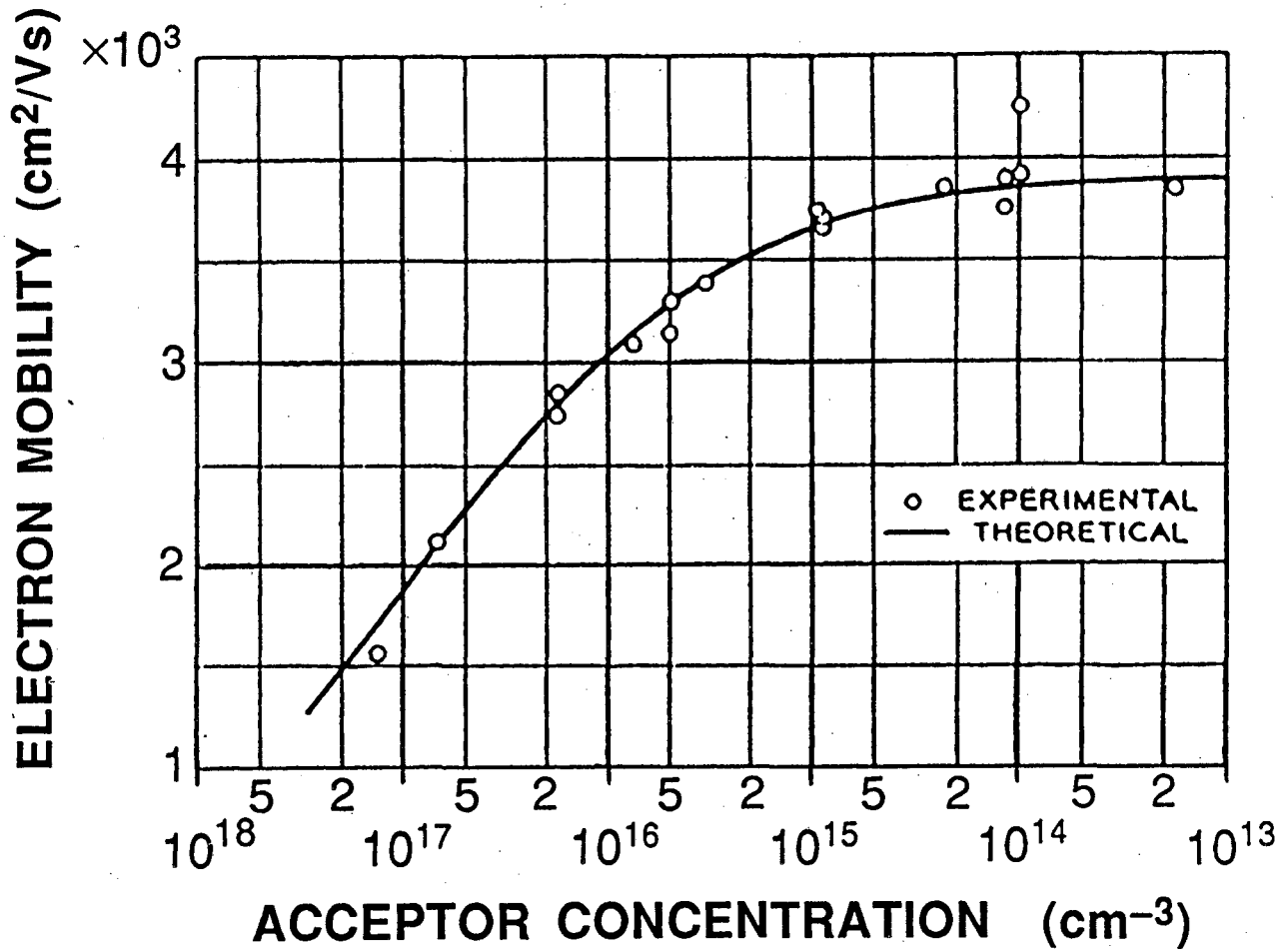
ELECTRON MOBILITY (cm²/Vs)
×10³
4
3
2
1
5 2 5 2 5 2 5 2 5 2
10¹⁸ 10¹⁷ 10¹⁶ 10¹⁵ 10¹⁴ 10¹³
ACCEPTOR CONCENTRATION (cm⁻³)
EXPERIMENTAL
THEORETICAL

Figure 10

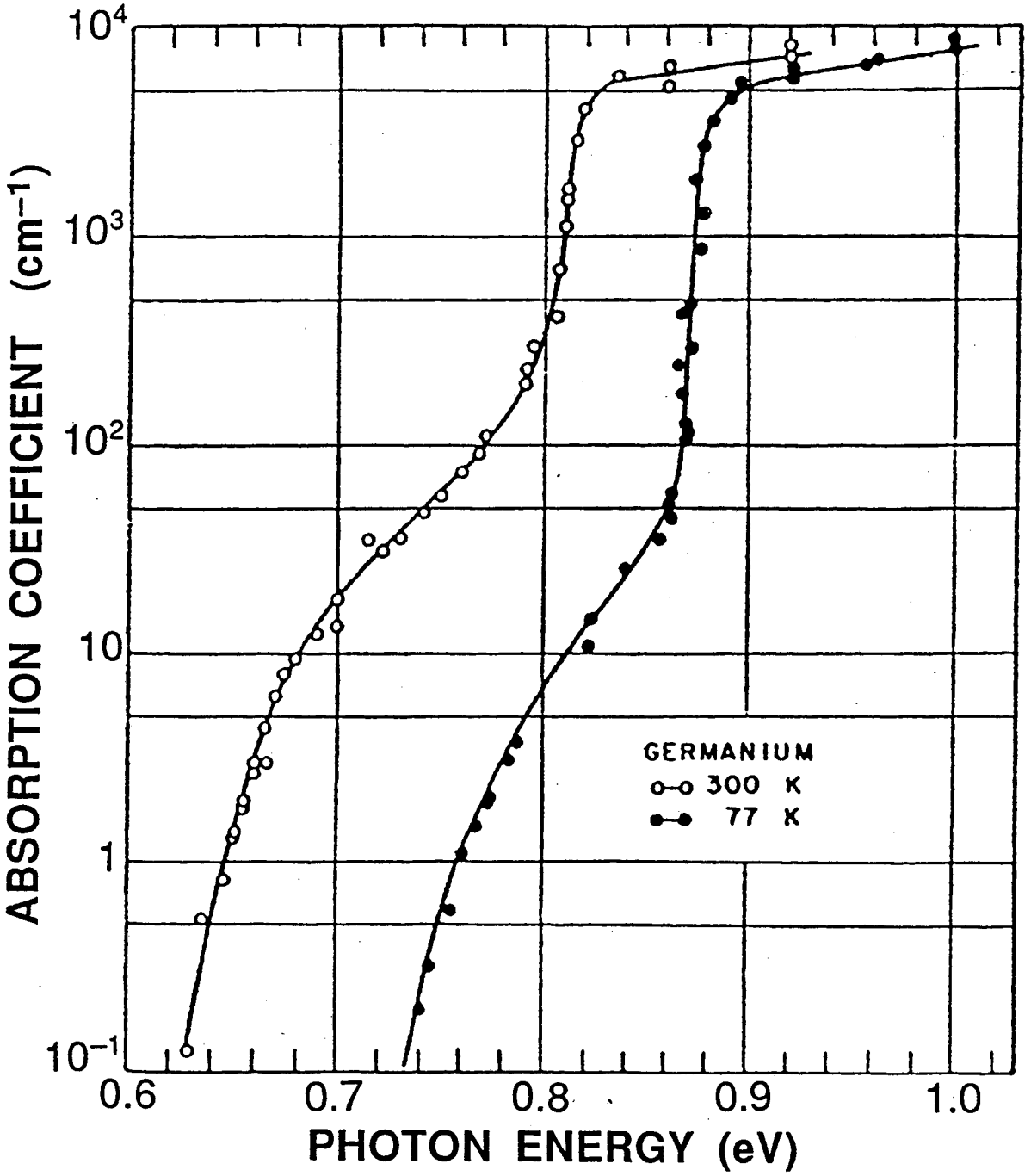
ABSORPTION COEFFICIENT (cm⁻¹)
10⁴
10³
10²
10
1
10⁻¹
0.6
0.7
0.8
0.9
1.0
PHOTON ENERGY (eV)
GERMANIUM
300 K
77 K

Figure 11

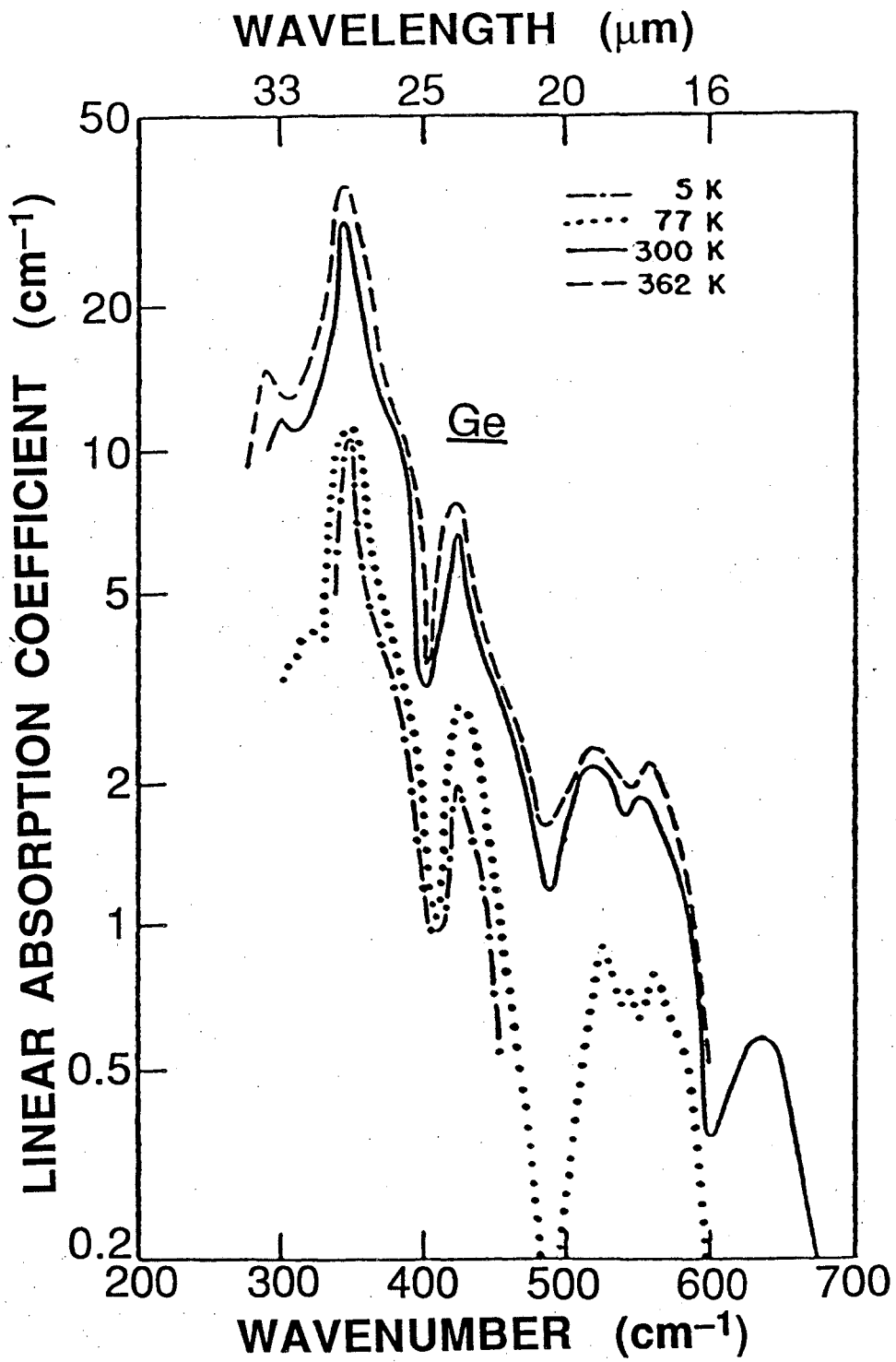
WAVELENGTH (μm)
33
25
20
16
50
20
10
5
2
1
0.5
0.2
LINEAR ABSORPTION COEFFICIENT (cm⁻¹)
5 K
77 K
300 K
362 K
Ge
200
300
400
500
600
700
WAVENUMBER (cm⁻¹)

Figure 12

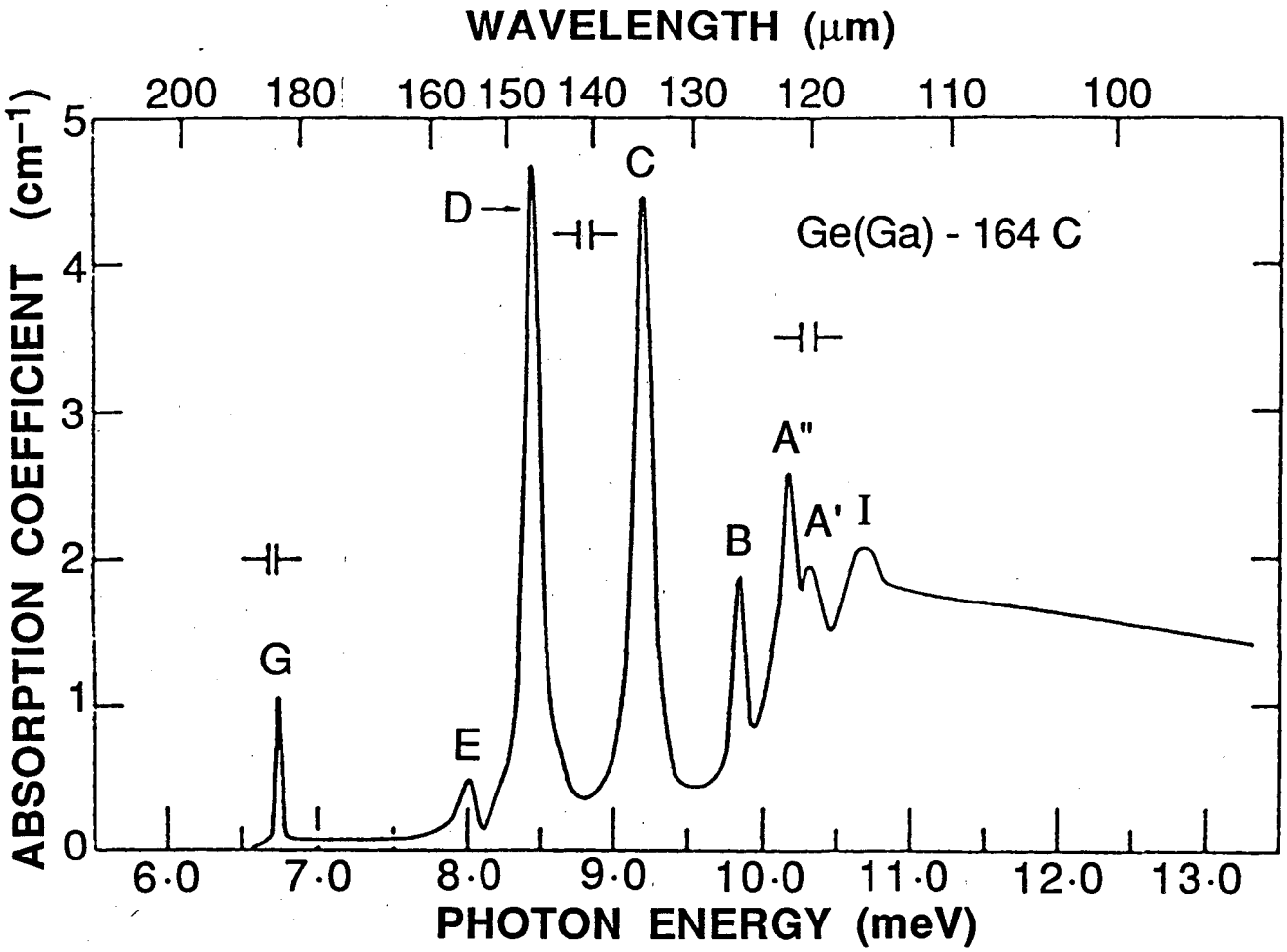
WAVELENGTH (μm)
200
180
160
150
140
130
120
110
100
ABSORPTION COEFFICIENT (cm⁻¹)
5
4
3
2
1
0
Ge(Ga) - 164 C
G
E
D
C
B
A"
A'
I
6·0
7·0
8·0
9·0
10·0
11·0
12·0
13·0
PHOTON ENERGY (meV)

Figure 13

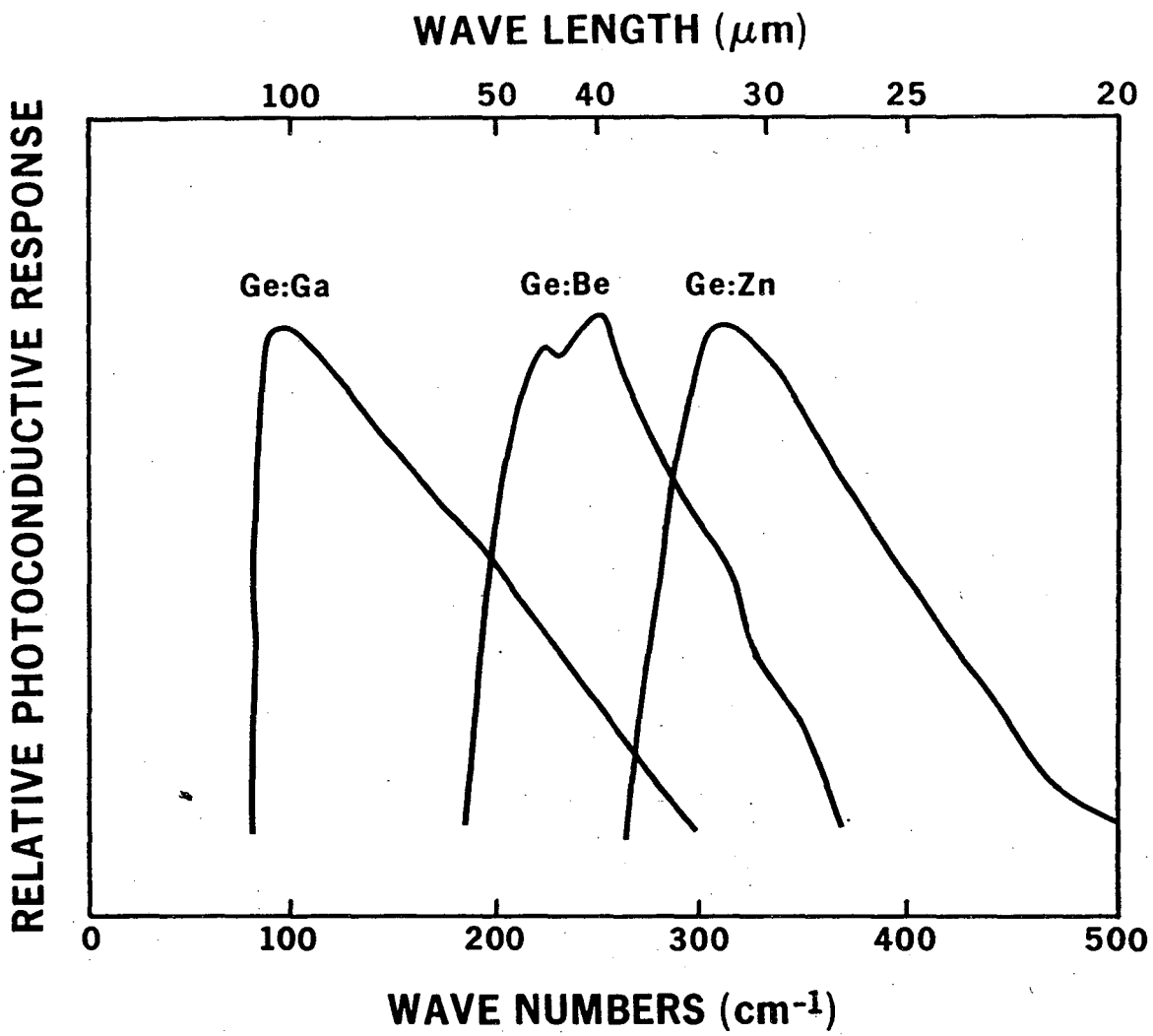

XBL 843-1141

Figure 14

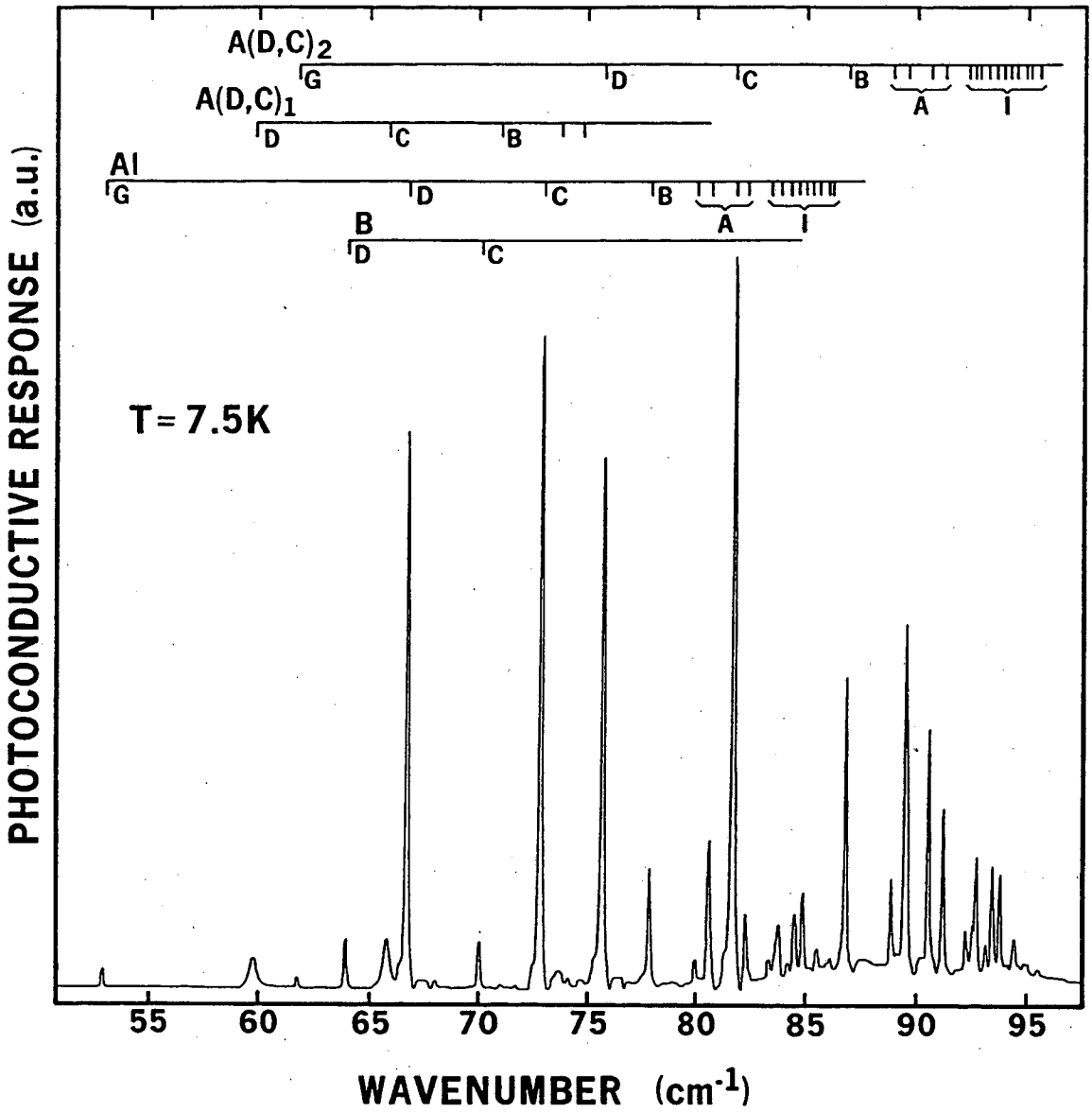

XBL 863-1160

Figure 15

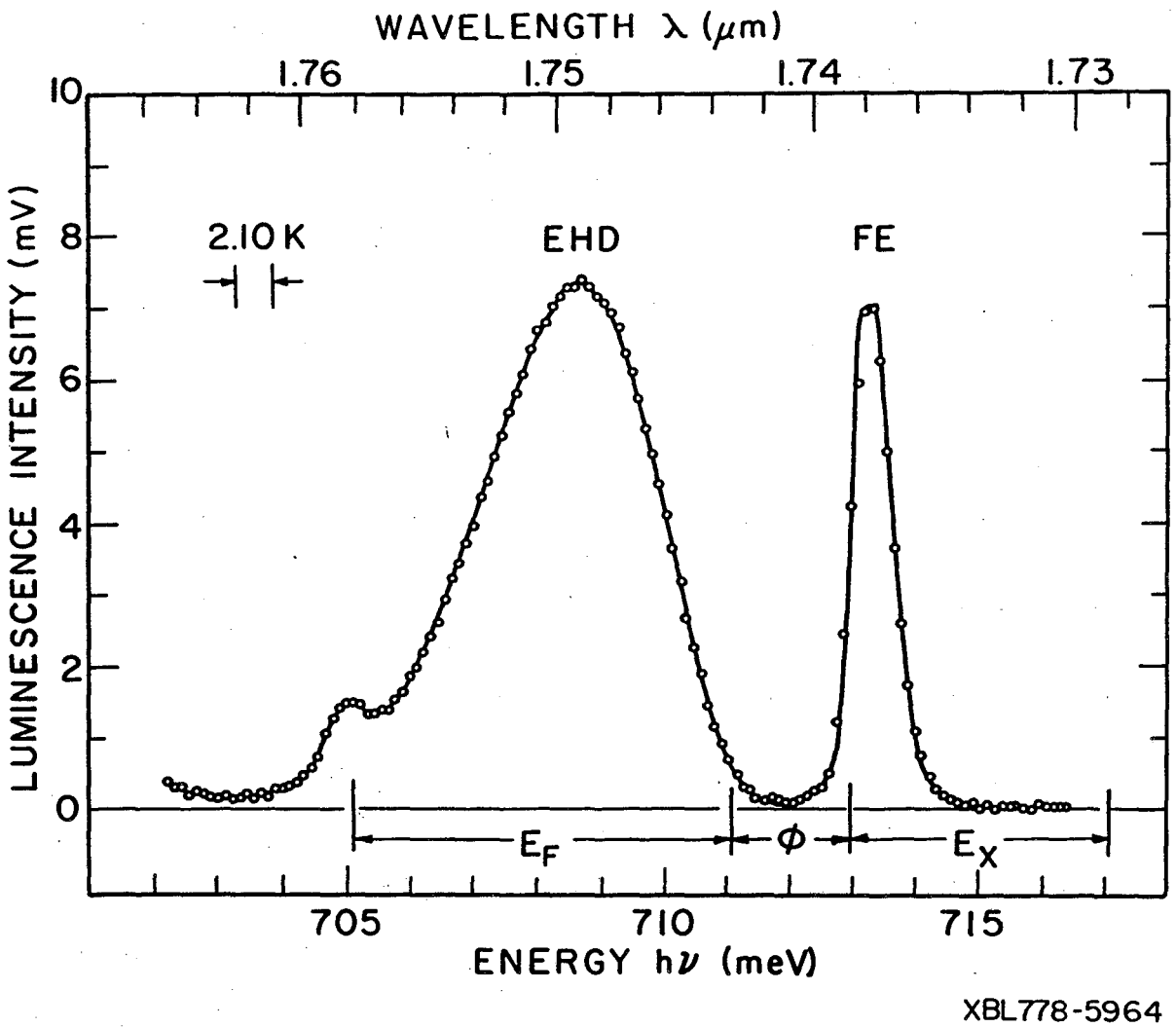
WAVELENGTH λ (μm)
1.76
1.75
1.74
1.73
10
8
6
4
2
0
LUMINESCENCE INTENSITY (mV)
2.10 K
EHD
FE
E_F
Φ
E_X
705
710
715
ENERGY hν (meV)
XBL778-5964

Figure 16

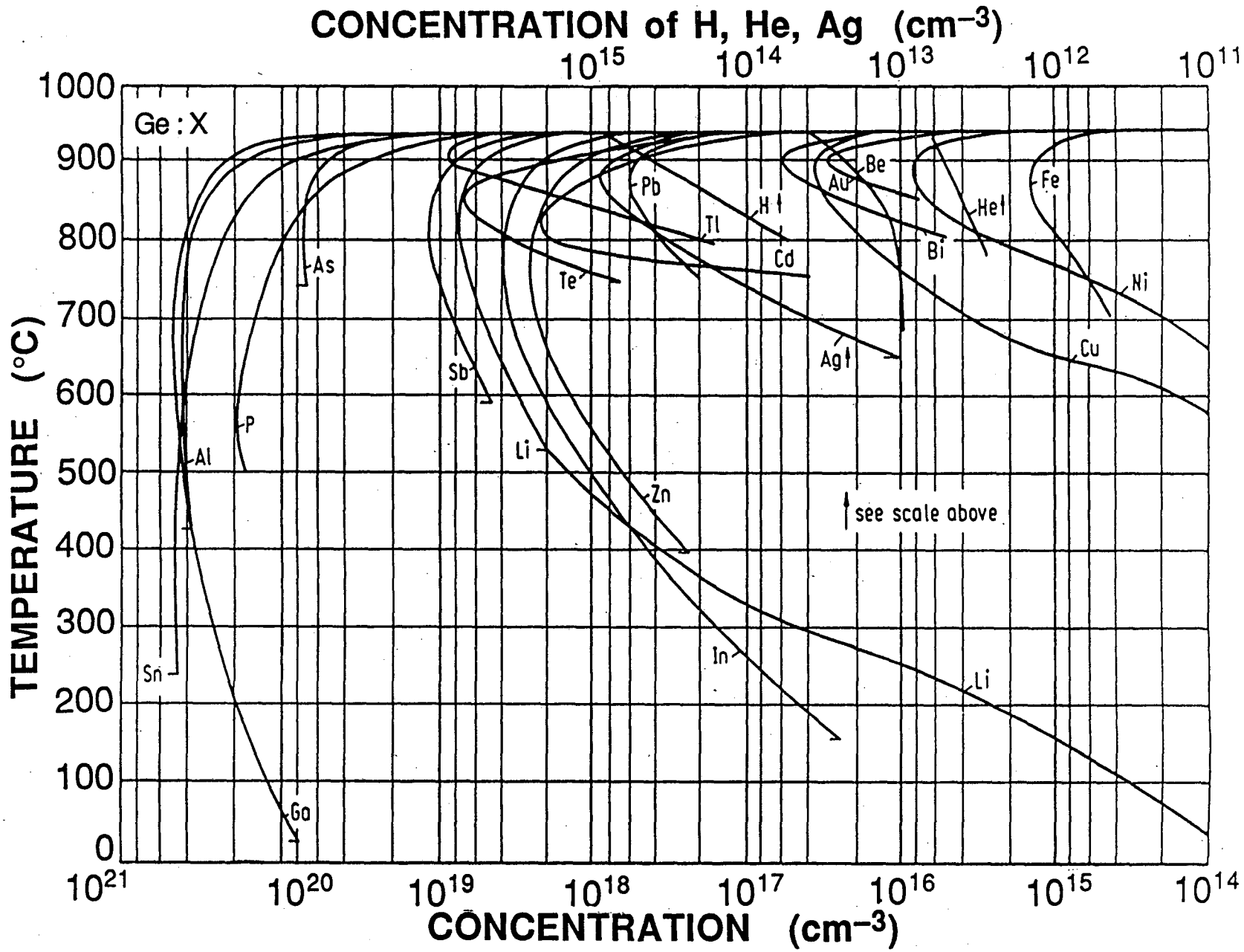
CONCENTRATION of H, He, Ag (cm^{-3})
10^{15}
10^{14}
10^{13}
10^{12}
10^{11}
Ge : X
TEMPERATURE (°C)
1000
900
800
700
600
500
400
300
200
100
0
As
P
Al
Sn
Ga
Sb
Li
Te
Pb
Tl
H
Cd
Zn
In
Ag
Au
Be
Bi
He
Fe
Ni
Cu
Li
see scale above
10^{21}
10^{20}
10^{19}
10^{18}
10^{17}
10^{16}
10^{15}
10^{14}
CONCENTRATION (cm^{-3})

Figure 17

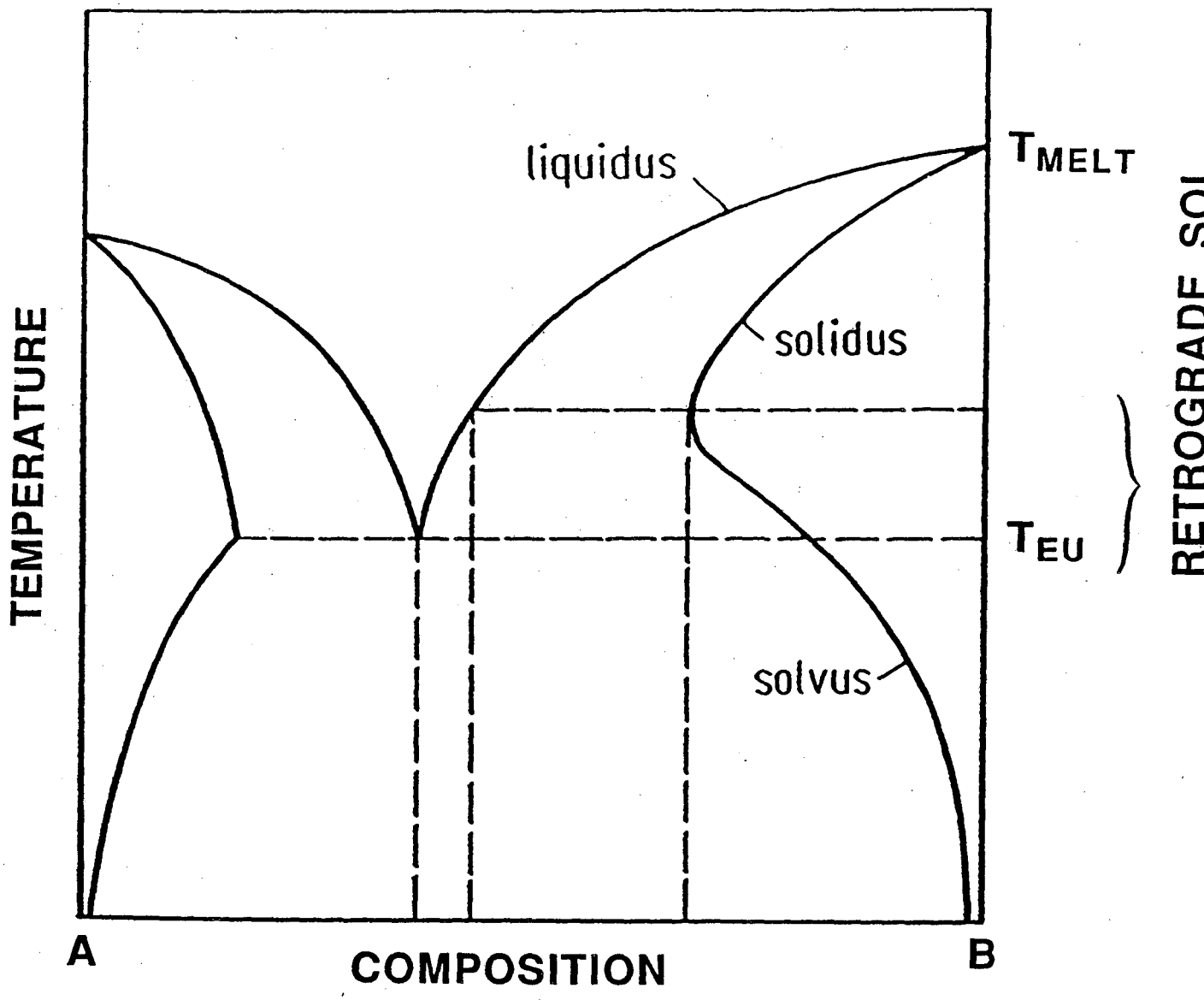
liquidus
T_{MELT}
solidus
TEMPERATURE
T_{EU}
solvus
A
COMPOSITION
B

Figure 18

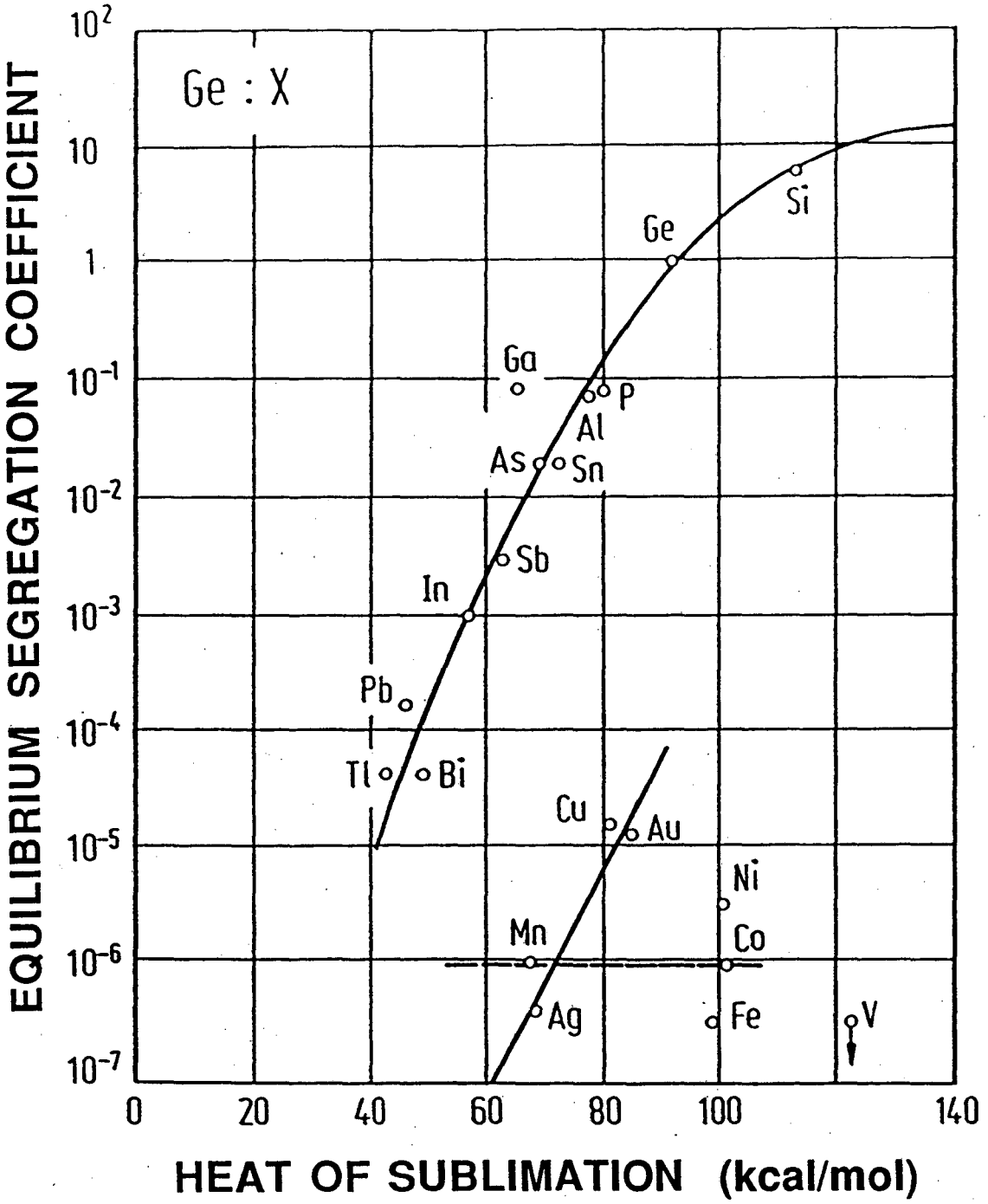
Ge : X
EQUILIBRIUM SEGREGATION COEFFICIENT
HEAT OF SUBLIMATION (kcal/mol)
10^2
10
1
10^{-1}
10^{-2}
10^{-3}
10^{-4}
10^{-5}
10^{-6}
10^{-7}
0
20
40
60
80
100
140
Si
Ge
Ga
P
Al
As
Sn
Sb
In
Pb
Tl
Bi
Cu
Au
Ni
Mn
Co
Ag
Fe
V

Figure 19

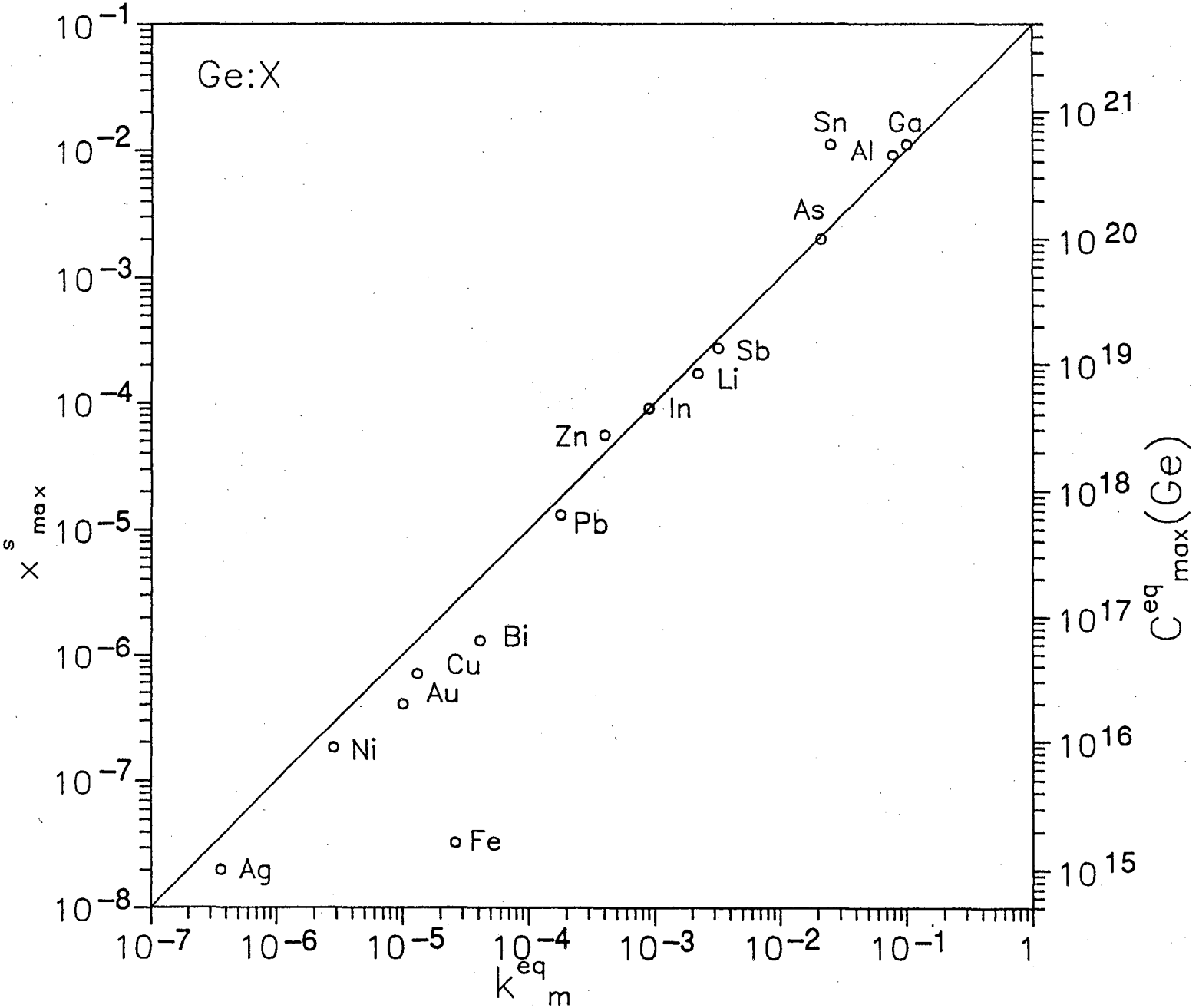
Ge:X
Sn
Ga
Al
As
Sb
Li
In
Zn
Pb
Bi
Cu
Au
Ni
Fe
Ag
10^{-1}
10^{-2}
10^{-3}
10^{-4}
10^{-5}
10^{-6}
10^{-7}
10^{-8}
X_s^{max}
10^{-7}
10^{-6}
10^{-5}
10^{-4}
10^{-3}
10^{-2}
10^{-1}
1
k_m^{eq}
10^{21}
10^{20}
10^{19}
10^{18}
10^{17}
10^{16}
10^{15}
$C_{max}^{eq}(Ge)$

Figure 20

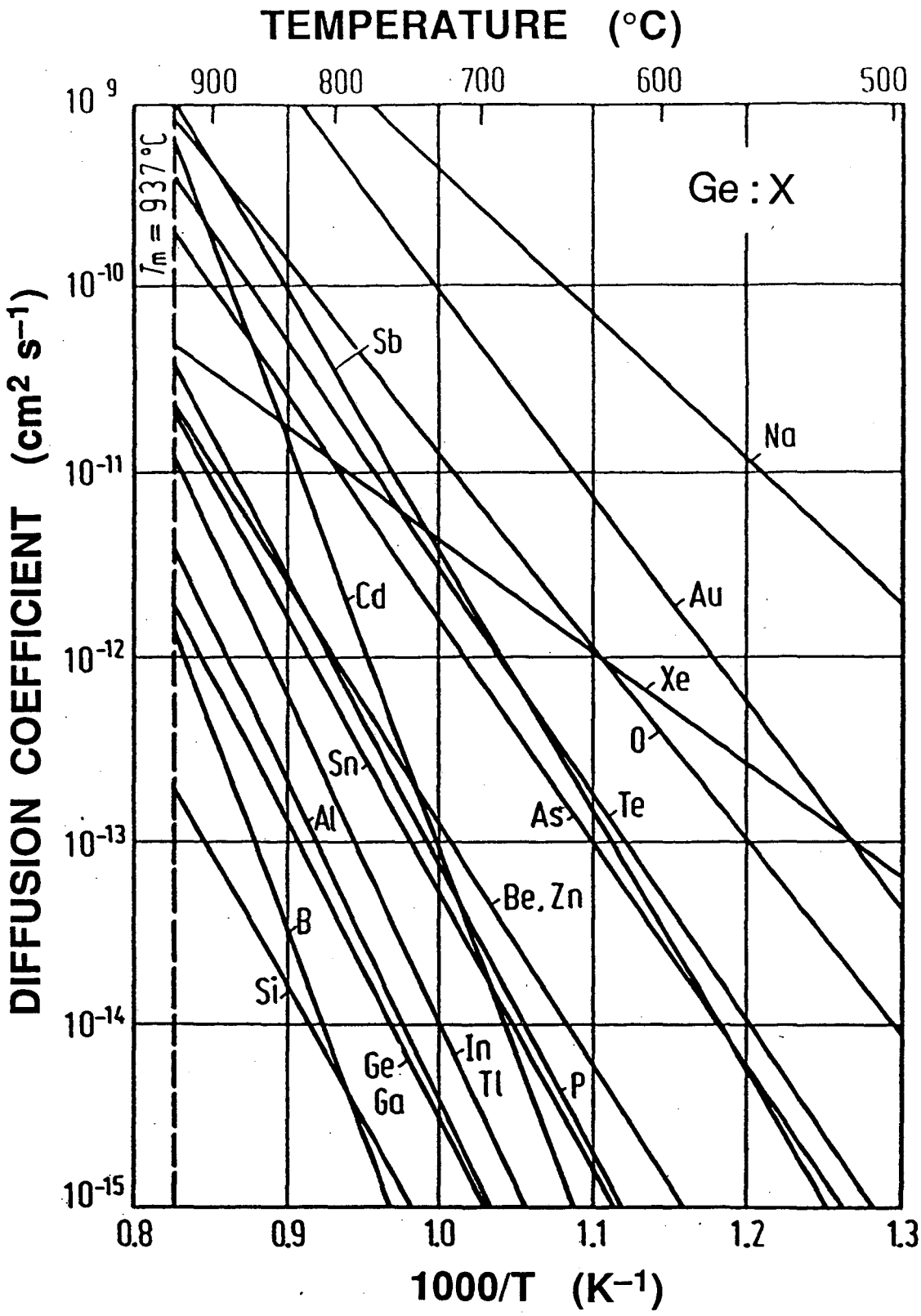
TEMPERATURE (°C)
900
800
700
600
500
Ge : X
T_m = 937°C
DIFFUSION COEFFICIENT (cm² s⁻¹)
10⁻⁹
10⁻¹⁰
10⁻¹¹
10⁻¹²
10⁻¹³
10⁻¹⁴
10⁻¹⁵
Sb
Na
Cd
Au
Xe
O
Sn
Al
As
Te
Be, Zn
B
Si
In
Tl
Ge
Ga
P
0.8
0.9
1.0
1.1
1.2
1.3
1000/T (K⁻¹)

Figure 21

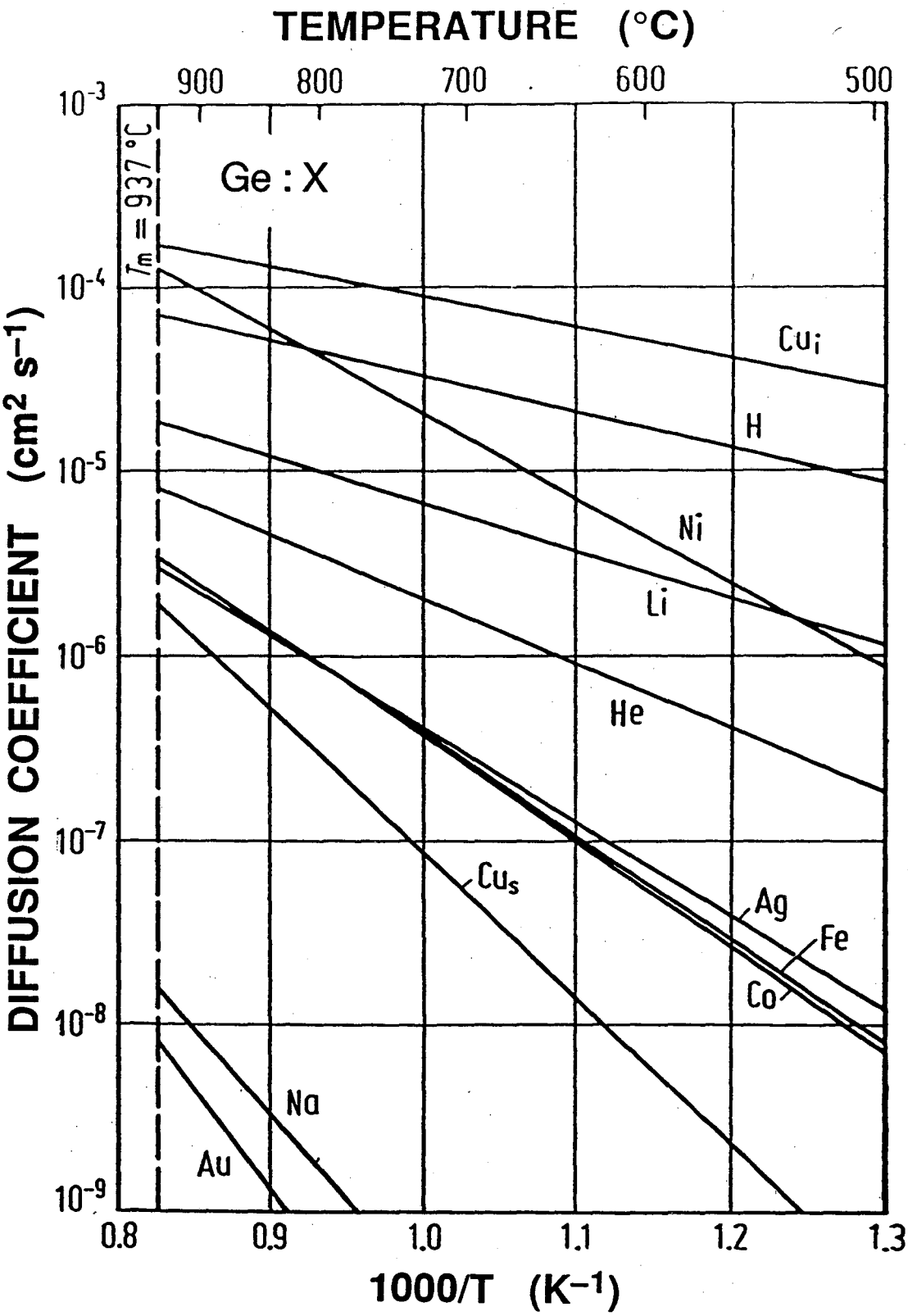
TEMPERATURE (°C)
900
800
700
600
500
Ge : X
T_m = 937 °C
DIFFUSION COEFFICIENT (cm² s⁻¹)
10⁻³
10⁻⁴
10⁻⁵
10⁻⁶
10⁻⁷
10⁻⁸
10⁻⁹
Cu_i
H
Ni
Li
He
Cu_s
Ag
Fe
Co
Na
Au
0.8
0.9
1.0
1.1
1.2
1.3
1000/T (K⁻¹)

Figure 22

LAWRENCE BERKELEY LABORATORY
UNIVERSITY OF CALIFORNIA
TECHNICAL INFORMATION DEPARTMENT
BERKELEY, CALIFORNIA 94720